HEAT AND CURRENT PROPAGATION IN BUFFERED SUPERCONDUCTING AND HYPER-CONDUCTING WIRE

THESIS

Jesse L. Lynn, Captain, USAF

AFIT/GAM/ENC/09-02

DEPARTMENT OF THE AIR FORCE
AIR UNIVERSITY

AIR FORCE INSTITUTE OF TECHNOLOGY

Wright-Patterson Air Force Base, Ohio

The views expressed in this document are those of the author and do not reflect the official policy or position of the United States Air Force, the United States Department of Defense or the United States Government.

AFIT/GAM/ENC/09-02

HEAT AND CURRENT PROPAGATION IN BUFFERED SUPERCONDUCTING

AND HYPER-CONDUCTING WIRE

THESIS

Presented to the Faculty

Department of Mathematics and Statistics

Graduate School of Engineering and Management

Air Force Institute of Technology

Air University

Air Education and Training Command

in Partial Fulfillment of the Requirements for the

Degree of Master of Science

Jesse L. Lynn, BA

Captain, USAF

10 December 2009

AFIT/GAM/ENC/09-02

HEAT AND CURRENT PROPAGATION IN BUFFERED SUPERCONDUCTING

AND HYPER-CONDUCTING WIRE

Jesse L. Lynn, BA
Captain, USAF

Approved:

_____	_____
Lt Col Kyle A. Novak (Chairman)	Date
_____	_____
Dr. William P. Baker (Member)	Date
_____	_____
Dr. George A. Levin (Member)	Date

AFIT/GAM/ENC/09-02

Abstract

This research models and analyzes the distribution of heat and current in a buffered superconducting or hyper-conducting wire that shows potential for use in different capacities in multiple Air Force systems including the Active Denial System. The thesis includes a brief background of the reaction-diffusion system of partial differential equations provided by AFRL/RZPG and development of the numerical scheme. It then explores solutions to the model. These solutions indicate some of the various heat-related failures that may be observed in such a wire. The nature of the solutions observed depends on the characteristics of the wire, operating temperature and efficiency of cooling.

Table of Contents

List of Figures

HEAT AND CURRENT PROPAGATION IN BUFFERED SUPERCONDUCTING AND HYPER-CONDUCTING WIRE

I. Introduction

Over the last two decades the Department of Defense has shifted its focus more and more towards peace keeping and addressing asymmetric threats. Along with this shift have come increased fighting in urban areas and a need to minimize collateral damage. There has consequently been an increased need for non-lethal weapons. In 2000 the Air Force began testing the Active Denial System, a less-than-lethal crowd control system utilizing a direct-able microwave beam. The Air Force is currently sponsoring work to develop an aerial variant of the Active Denial System for use on helicopters.

Active Denial and similar systems require large amounts of power. In order to generate large, megawatt-level amounts of electrical power, either high voltage or large levels of current need to be available. Voltage is limited at higher altitudes due to lower atmospheric pressure [5]. Voltages that are considered low at sea level will produce arcing at higher altitudes. For that reason, the way to increase power on an aircraft is not to increase voltage but to increase current. An increase in current will require larger gauge and/or more wiring. For small aircraft, two major concerns are the size and weight of a prospective system. Power generation and transport could be accomplished with conventional copper wires on a C-130, where weight is not as much of an issue. Conventional power production and transport at megawatt levels would be too heavy and bulky to be used on a smaller platform, such as a helicopter. In order to develop a helicopter mounted Active Denial System, several components

need to be smaller and lighter than their ground counterparts.

A high-temperature superconducting wire is considerably smaller and lighter than a comparable capacity copper wire. In terms of weight, even when cryogenics systems are factored in, high-temperature superconductors have shown potential savings of roughly 100 kg/m of cable operating at 10 to 15 MW DC [5]. This makes high-temperature superconductor-based components a promising option for use in the spatially limited environment of a helicopter or other aircraft.

Reliability is a concern for any military system and a crucial part of reliability is survivability. In high-temperature superconductors, one of the survivability requirements is temperature remaining below a damage threshold. At this temperature the superconductor will be irreversibly damaged. This constitutes a failure of the system. To prevent a failure, it is necessary to be able to detect as quickly as possible, by voltage drop or temperature variance, any heat pockets that may develop and act to mitigate them. Figure 1 shows a burned out armature from a liquid-hydrogen cooled generator. The windings of the armature are copper, but the rotors of the generator were high-purity aluminum which is a hyper-conductor. The burned portions of the armature illustrate the severity of the damage caused by such failures.

In current, state-of-the-art, high-temperature superconducting wires, the temperature may climb in a localized region and not be detectable until the system fails due to damage from heat [9]. The Power Generation Branch of the Power Division, Propulsion Directorate, Air Force Research Laboratory (AFRL/RZPG) is researching buffered high-temperature superconductors and the impact of varying interfacial resistivity between conducting layers.

This research addresses a general model for current and temperature in a superconducting wire and the effect of increasing interfacial resistivity between conducting layers. The intent is to increase the rate at which heat will spread so that it is detected

Figure 1. The armature from a liquid-hydrogen cooled generator. The rotors of the generator were high-purity aluminum which is a hyper-conductor. The windings of the armature are copper. Note the burned areas visible on the facing edge of the armature [7].

before the damage threshold is reached. While damage or destruction of the system is the most dramatic type of heat related failure, there are other less severe types of failure that may be observed. The range of failures from destruction of the system to minor interruption of current will be examined. The final possibility addressed is a system that will recover from a heat related incident and maintain stable operation.

Chapter 2 discusses relevant background and presents the model as a reaction-diffusion system. Equilibrium solutions are explored and basic dimensional analysis is performed on the system. Chapter 3 develops a fast, robust implicit/explicit numerical scheme for the model. Chapter 4 presents solutions of the reaction-diffusion system as interfacial resistance and coefficient of cooling are varied. The solutions are qualitatively separated into five classes according to morphological behavior. Chapter 5 discusses areas for future research.

II. Background

2.1 Superconductors

Superconductivity, discovered in 1911, is a property displayed by certain materials that provide very low (or no) electrical resistance as well as excluding magnetic fields at low temperatures. Over the years several different materials, originally metals but later ceramics and organic materials, have exhibited superconductivity [12]. Superconductors are currently used in applications ranging from magnetic resonance imaging to particle accelerators, primarily as high-field electromagnets.

In a superconductor, at a certain temperature called the *critical temperature*, there is a sudden change from zero electrical resistivity to high electrical resistivity as temperature increases. In yttrium barium copper oxide (YBCO) for example, this transition takes place over a 2 K span. Figure 2 on page 6 [12] illustrates the change in resistivity as a function of temperature for YBCO. While there are several ways to classify superconductors, for the purposes of this research the distinction of high or low temperature superconductors is sufficient.

$YBa_2Cu_3O_{7-\delta}$ is a ceramic that was one of the first materials to display superconductivity at a temperature higher than 77 K, the boiling point of liquid nitrogen. It is a semiconductor, but for certain values of $\delta \in [0, 1]$ it becomes a superconductor. Its superconducting characteristics vary considerably depending on concentration of oxygen with critical temperature ranging from about 28 K to 92 K. Figure 2 shows a plot of electrical resistivity as a function of temperature. For $\delta = 0.22$, the critical temperature is about 77 K and for $\delta = 0$, the critical temperature jumps to about 92 K. In addition to high critical temperature, YBCO has been shown to be more robust than other superconductors with regard to maintaining superconductivity in the presence of nearby magnetic fields, having been observed to maintain supercon-

ductivity at low temperature in fields higher than 100 T (100 Tesla) [15]. Even at approximately 75 K the critical field of YBCO is in the neighborhood of 50 T [12]. When δ is greater than about 0.7, YBCO becomes strictly semi-conducting [12]. Unless specifically referring to δ values, optimally-prepared (highest oxygen with $\delta = 0$) $YBa_2Cu_3O_{7-\delta}$ will be referred to as YBCO in the sequel. Other superconducting materials have different critical temperatures, but they all display an abrupt change from zero resistivity to high resistivity as the temperature transitions through the critical temperature.

Low-temperature superconductors operate in temperature ranges less than about 23 K. This means that a typical cooling method involves liquid helium which boils at roughly 4 K. Such a cooling system is expensive and bulky. Low-temperature superconductors are also highly susceptible to heat and magnetic fields. This limits the range of applications for which they are suited and makes them unsuitable for most military applications.

If the temperature of a superconducting material rises above its critical temperature or if a local magnetic field becomes too powerful, the material loses its superconducting capability. This process is called *quench* and at that point the superconductor may be damaged or destroyed unless appropriate protective measures are in place. When a superconductor quenches, a region called a *normal zone* is created where there is greater than zero electrical resistance [7]. The normal zone will spread as the temperature in that region rises heating adjacent regions to quench. In low-temperature superconductors, *normal zone propagation* occurs fast enough that quench can be detected and mitigated—typically by shutting down the system to restore temperature—before the temperature reaches the damage threshold. The low operating temperature and susceptibility to magnetic fields makes them, generally, suitable for a narrow range of real world applications where conditions can be carefully
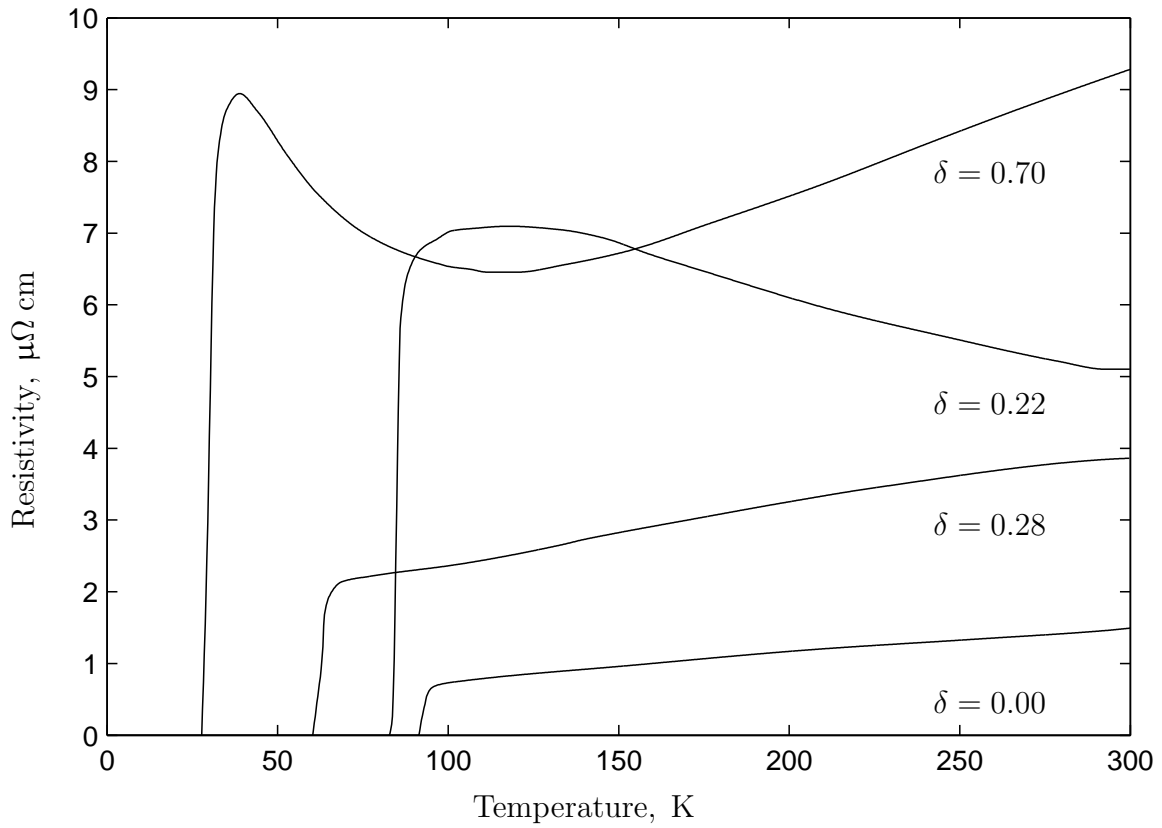
Figure 2. **Resistivity as a function of temperature for different values of parameter** δ **in YBa$_2$Cu$_3$O$_{7-\delta}$ [12].** **Notice the rapid shift from superconducting to electrically insulating as temperature increases.**

controlled and space is not a limiting factor, such as an MRI in a hospital.

2.2 High-Temperature Superconductors

High-temperature superconductors maintain zero electrical resistivity up to approximately 135 K. This means that liquid nitrogen which boils at about 77 K can be used to cool these materials. This makes high-temperature superconductors more suitable for many applications. Unfortunately, normal zone propagation is sufficiently slow in high-temperature superconductors that temperature can reach the damage threshold before there is any indication of quench [9]. This makes quench difficult to detect and potentially harder to mitigate.

A superconductor may be coupled with a conventional conductor to help prevent damage/destruction brought on by quench. In this case the electrical current which ideally travels through the superconducting material simply reroutes through the conventional conductor until heat dissipation restores low temperature or the system can be shut down.

There is some small amount of electrical resistance between the superconducting and normal conducting layers. Traditionally, it has been thought that this *interfacial resistance* needs to be small [9]. AFRL/RZPG is currently investigating the effect of increasing interfacial resistance on the speed of normal zone propagation. If the speed of normal zone propagation could be made fast enough to allow detection and shutdown prior to system damage, then high-temperature superconductors could be used in a variety of military applications including the electromagnets used for microwave generation in the Active Denial System.

2.3   Development of the Model from Physical Principles

The superconducting wire is a ribbon 4 mm wide composed of four layers as illustrated in Figure 3. The first layer is a substrate approximately 50 μm thick. This substrate is made out of stainless steel, nickel, or Hastelloy (a high-performance alloy). A layer of YBCO approximately 1 μm thick is deposited on the substrate and a thin (nanometers thick) resistive layer may be deposited on top of this. The final layer is 50 μm of copper which acts as a stabilizer by providing an alternate route for current to travel if the temperature rises above the critical temperature of the YBCO and the YBCO loses its superconductivity [9].

For the sake of a mathematically tractable solution, a simplification made to the mathematical model is the reduction of a three-dimensional wire to a one-dimensional model. This is reasonable because the thickness and width of the wire are small enough that heat can be considered approximately uniform in those directions [9]. Readers interested in the complete development of this model should refer to [9]. The development in this thesis focuses on the elements of the physical model that cannot be passed over without loss of context. The physical phenomenon in question
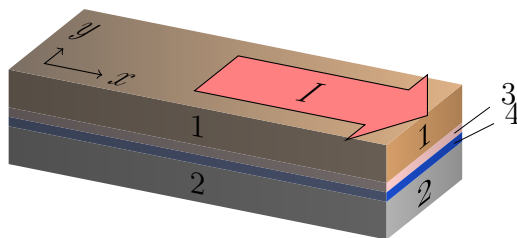
Figure 3. Cross-sectional representation of the buffered ribbon wire. 1 represents the copper which acts as a stabilizer allowing current to flow when superconductivity is lost. 2 represents the Hastelloy substrate which provides a base for depositing the YBCO. Because of the relatively high resistance of the Hastelloy compared to the copper or the YBCO, no current flows through the Hastelloy. 3 represents the thin resistive layer providing interfacial resistance between the YBCO and the copper. 4 represents the YBCO.

is described by a system of partial differential equations:

$$\frac{\partial}{\partial t}\theta(x,t) = \frac{\partial^2}{\partial x^2}\theta(x,t) + (u(x))^2 + f(\theta(x,t))(1 - (u(x)))^2 \cdots$$

$$+ r(x)\left(\frac{\partial}{\partial x}u(x)\right)^2 - \kappa(\theta(x,t) - \theta(x,t)_0)$$

$$\frac{\partial}{\partial x}\left(r(x)\frac{\partial}{\partial x}u(x)\right) = u - f(\theta(x,t))(1 - (u(x)))$$

For readability, this system will be written as

$$\theta_t = \theta_{xx} + u^2 + f(\theta)(1 - u)^2 + r(u_x)^2 - \kappa(\theta - \theta_0) \tag{1}$$

$$(r(u)_x)_x = u - f(\theta)(1 - u). \tag{2}$$

In either case, the first equation describes heat and the second describes current in the wire presented previously. The variables and parameters in the above system are listed in Table 1 on page 11. All terms are dimensionless in this model. In practice the operating temperature θ is greater than the temperature of the coolant θ_0. The critical temperature of the superconductor is defined to be $\theta = 0$, so in the absence of a failure the operating temperature will be negative. This means the coolant temperature, for obvious physical reasons lower than any other temperature in the model, is always a negative number. The fraction of total current that travels through the stabilizer u is a number between zero and one, that is $u \in [0, 1]$, with $u = 0$ denoting all current flows through the superconductor and $u = 1$ indicating all current flows through the stabilizer.

Following the development in [8, 9], the first terms in (1) $\theta_t = \theta_{xx}$ are the basic heat equation. This provides diffusion in the model. The following three terms $u^2 + f(\theta)(1 - u)^2 + r(u_x)^2$, which are positive, contribute heat. The u^2 term represents the heat produced by current flowing through the stabilizer. Notice when temperature

9

is low enough, there is no current traveling through the stabilizer and this term will not contribute any heat. The $f(\theta)(1-u)^2$ represents the heat produced by the current in the superconductor. When temperature is low, this will contribute little-to-no heat because $f(\theta)$ will evaluate to zero, or nearly zero. The function $f(\theta)$ is detailed in the following section. When all current is passing through the stabilizer this term will not contribute heat. The final heat building term $r(u_x)^2$ represents the heat produced by current crossing the interface between the superconductor and the stabilizer. Recall the resistive layer between the superconductor and the stabilizer. This resistance r is not constant, for reasons that will be detailed below. The coefficient of cooling κ is multiplied by the difference between operating and coolant temperature $\theta - \theta_0$ and together they represent the heat loss and cooling forces. The second equation, essentially Poisson's equation, derives from the condition of charge conservation across the vertical thickness of the wire. The right hand side, similar to the first equation, comprises a term for current through the stabilizer u, and a term for current through the superconductor $f(\theta)(1-u)$.

For the superconducting wire, θ is dimensionless temperature derived from the following relationship (variables are defined in Table 1):

$$\theta = \frac{T - T_1}{T_c - T_1} \tag{3}$$

The current sharing temperature T_1 can be thought of as the temperature at which current starts to flow through the stabilizer. It is below the critical temperature and is detailed in [9]. The domain is given by $x \in [-L, L]$, L is dimensionless, with either reflecting or periodic boundary conditions. Reflecting, or thermally insulating, boundary conditions model a wire of length $2L$, while periodic boundary conditions model a closed loop of wire. Mathematical representations of the boundary conditions are presented in the following chapter. The interfacial resistance along the ribbon is

Table 1. Variables and Terms for Equations 1 and 2

T_c	critical temperature
T_1	current sharing temperature
T	temperature
T_0	ambient (coolant) temperature
κ	coefficient of cooling (dimensionless)
θ	dimensionless temperature
θ_0	dimensionless ambient temperature
$f(\theta)$	transition function
r	interfacial resistance (dimensionless)
u	fraction of current through copper stabilizer (dimensionless)
t	time (dimensionless)
x	length (dimensionless)

given by $r(x)$. Typically, $r(x)$ is a constant r_0 along the length of the ribbon, but near the ends it is beneficial to reduce resistivity for the purpose of simulating the wire accurately. In the wire, current enters the wire through the copper stabilizer. Current will need to overcome the interfacial resistance in order to flow into the superconductor. To make sure this happens, resistance is minimized at each end of the wire. To model this

$$r(x) = \epsilon + r_0 \left(1 - e^{(\cos(x\pi/(2L))^2/c^2} \right)$$

where $\epsilon = 0.01$, and $c = 0.1$. This modification is included in the model with reflecting boundary conditions. It is not used in the model with periodic boundary conditions. In that case interfacial resistance is held constant $r(x) = r_0$ in the entire domain. This allows current and temperature to pass from L to $-L$ (through the boundary) without interference. In this way, the periodic boundary conditions simulate a length of wire with uniform activity at fixed intervals.

2.4 Transition Functions

Of particular interest in the study of this system is the function that models the transition of the superconductor from zero to high electrical resistance. This is represented in the system by $f(\theta)$. A peculiarity of superconducting materials is the rapid, or immediate, transition from zero electrical resistance to high electrical resistance at the critical temperature. Below the critical temperature the current traveling through the stabilizer will be low $u \approx 0$. As the operating temperature climbs, current through the stabilizer will increase until $u = 1$ and there is no current moving through the superconductor. To properly model this, three functions have been considered as the *transition function* describing electrical resistivity ρ of the superconductor. The first, and simplest, is the scaled Heaviside function

$$f(\theta) = \Gamma H(\theta - 1) = \begin{cases} 0 & \text{if } \theta < 1 \\ \Gamma & \text{if } \theta \geq 1 \end{cases} \qquad \text{where } \Gamma \gg 1.$$

As shown in Figure 4, this is a step function which equals zero below the critical temperature and a constant at or above the critical temperature.

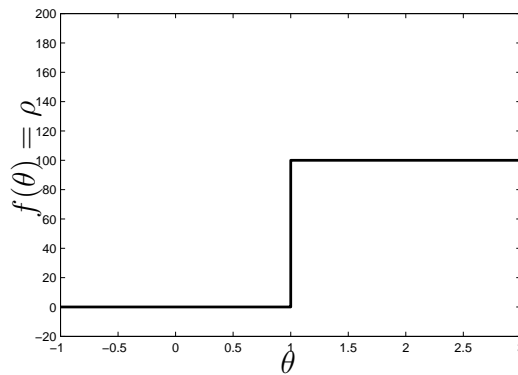The next function considered is the variable ramp shown in Figure 5. Although

Figure 4. Scaled Heaviside function for resistivity ρ as a function of temperature θ.

shown with a small Δ, in practice this will be variable depending on u and θ

$$f(\theta; u) = \begin{cases} 0 & \text{if } \theta < u \\ \Gamma(\theta - u)/(1 - u) & \text{if } u < \theta \leq 1 \\ \Gamma & \text{if } 1 < \theta. \end{cases}$$

The ramp models a finite (2 K) change between superconducting and insulating. This function has been used to describe the superconducting relation in the aforementioned buffered YBCO wire [8].

The final function considered is the exponential function

$$f(\theta) = e^{\theta}.$$

While the exponential function provides a smooth transition from low to high electrical resistivity, it is not as appropriate for the accurate modeling of the superconducting material. However, this model does describe a relevant and related physical device such as a ribbon wire of high purity aluminum and Hastelloy separated by a resistive layer of oxidized aluminum. The Hastelloy could be the same as that used in the
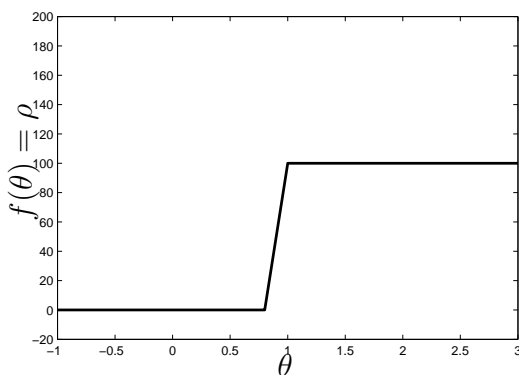

Figure 5. The ramp transition function for resistivity ρ as a function of temperature θ. Note, the ramp function has been fixed for readability. In practice, the slope of the ramp is variable.
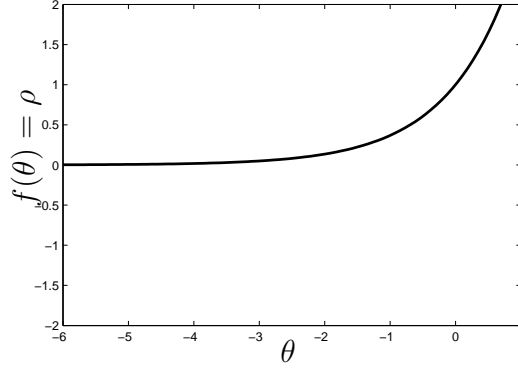
Figure 6. The exponential transition function for resistivity ρ as a function of temperature θ.

buffered YBCO wire, with a thin (a couple of nanometers thick) layer of aluminum deposited and allowed to oxidize in the air. Deposited on top of that would be a layer of high purity aluminum. Pure aluminum (at least 99.99% pure) is a hyperconductor. This means that its electrical resistivity is close to zero at sufficiently low temperatures [3]. Unlike superconductors, this change in resistivity is gradual, ranging from 7.55×10^{-4} $\mu\Omega$ cm at 20 K to 2.733 $\mu\Omega$ cm at 300 K [3]. Figure 7 on page 16 shows the relative electrical resistances of aluminum, Hastelloy, copper and YBCO. Notice that while aluminum's resistance gets very close to zero, it does so over a large temperature range, unlike the change in resistance of YBCO. The dimensionless temperature for a hyper-conducting wire made of high-purity aluminum and Hastelloy is slightly different than that of a superconducting wire. The dimensionless temperature θ is given by

$$\theta = \frac{T - T_1}{\Delta T}. \tag{4}$$

ΔT is used here because there would not be a critical temperature T_c in the hyper-conducting wire, instead there is only a *current sharing temperature* T_1 [7]. Unlike a superconductor, the temperature at which the resistance of aluminum becomes lower than that of Hastelloy is entirely determined by their relative thickness. For example, consider a wire such that the current sharing temperature $T_1 = 65$ K. The

electrical resistivity of aluminum at that temperature is $\rho_{\text{Al}} = .1384$ μΩ cm [3]. Since Hastelloy's electrical resistivity is 130 μΩ cm, the thickness of the Hastelloy would be need to be roughly one thousand times that of the aluminum. The temperature driven increase in resistance of aluminum, and the corresponding shift in current, is similar to what happens in the superconducting wire. In the superconducting wire the electrical resistance of the YBCO is zero when $T < T_c$ and current will flow through the YBCO. When $T > T_c$, resistance in the YBCO will be much higher than resistance in the copper. At that point, the current will overcome the interfacial resistance between the copper and the YBCO, transfer to the copper and continue flowing through the copper unless the temperature drops again. Figure 7 shows the change in resistance as a function of temperature for YBCO, high-purity copper, Hastelloy and high-purity aluminum. For readability, the electrical resistance of Hastelloy is shown for Hastelloy one hundred times as thick as the aluminum. In this case, widths of all materials are equal as are lengths. Also, the resistance of YBCO is shown at one-twentieth of actual for comparison to the resistance of copper.

Empirical observations suggest the specific function is not critical so long as it provides a change from zero or near zero resistivity to high resistivity over a narrow temperature range. In the physical wires and in the models the current will travel through the superconductor or the hyper-conductor so long as the temperature is low enough to allow it. Once the temperature passes the critical temperature, the YBCO—or the hyper-conductor—becomes a resistor and the current will reroute through the stabilizer (copper or Hastelloy, respectively). For this reason this thesis will address the case of the exponential function as transition function.
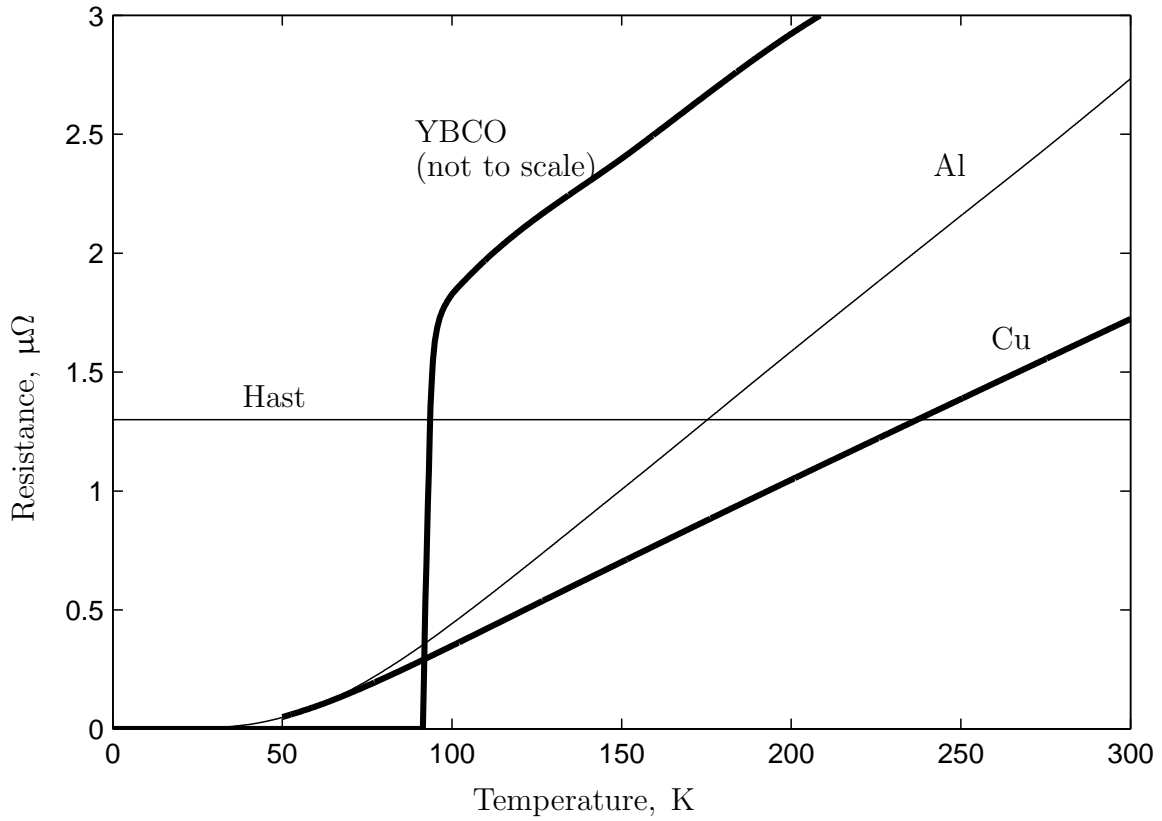
Figure 7. Resistance as a function of temperature for Hastelloy, YBCO, aluminum and copper [3, 12, 14]. Resistance of YBCO at $1\,\mu m$ thickness is shown as 5% of the actual resistance. Aluminum and copper are $50\,\mu m$ thick. Hastelloy must be 100 times thicker than the others to achieve comparable resistance. All materials are the same width, as they would be in a wire. Note that resistivity data for copper terminates at $50\,K$, while resistivity data for aluminum was available down to low temperature.

2.5   Constant Equilibrium Solutions

Prior to numerical modeling, it is necessary to develop a fundamental understanding of the solutions to the equilibrated system. Recall the system of equations for temperature θ and current u:

$$\theta_t = \theta_{xx} + u^2 + f(\theta)(1-u)^2 + r(u_x)^2 - \kappa(\theta - \theta_0)$$

$$(ru_x)_x = u - f(\theta)(1-u)$$

As an initial exploration of this system, a good starting point is determining the stable or constant equilibrium solutions. Consider current and temperature constant. Then $u_x = 0$, $\theta_x = 0$, $\theta_t = 0$, and $\theta_{xx} = 0$:

$$0 = u^2 + f(\theta)(1-u)^2 - \kappa(\theta - \theta_0) \tag{5}$$

$$0 = u - f(\theta)(1-u) \tag{6}$$

Now, solving (6) for u:

$$u = \frac{f(\theta)}{1 + f(\theta)}. \tag{7}$$

To find the equilibrium solutions, substitute (7) into (5) and simplify.

$$\kappa\left(\theta - \theta_0\right) = \frac{f(\theta)}{1 + f(\theta)}. \tag{8}$$

The solutions to (8) will depend on κ. These solutions are shown in Figure 8(a) on page 19 as well as Figures 8(b) and 9(a), where current u is a function of temperature θ. In those figures, the left and right hand side of (8) are plotted representing cooling forces and heating forces respectively. The solutions are indicated at the intersections or equilibrium of the cooling and heating terms. If temperature θ is greater than a

nearby constant equilibrium solution, then cooling will be stronger than the heating forces and θ decreases to converge to the equilibrium solution. On the other hand, if θ is less than a solution, the heating forces will be greater than the cooling and θ will increase to converge to the solution. Therefore these solutions are stable with regard to perturbations in temperature. In all of the above referenced figures, the low temperature equilibrium occurs at the ambient temperature for the system θ_0. In the adiabatic case, where $\kappa = 0$, there will be one solution and it will be a stable solution. Any introduction of heat (perturbation of the system) will cause a shift to the normal conducting regime and temperature will grow unbounded. In later instances, the largest value of κ for which there is a high-temperature equilibrium solution will be referred to as $\kappa^\star$. When $0 < \kappa < \kappa^\star$, there will be two stable equilibrium solutions a high-temperature and a low-temperature solution. When $\kappa^\star < \kappa$ there will only be a low-temperature solution. In Figure 9(b) showing solutions in the $\kappa\theta$-plane, one can see that for $\kappa = 0.06$ there would be three intersections. The highest of these intersections corresponds to the highest temperature of a solution to this system, $\theta_{\max}$ for the considered value of κ.
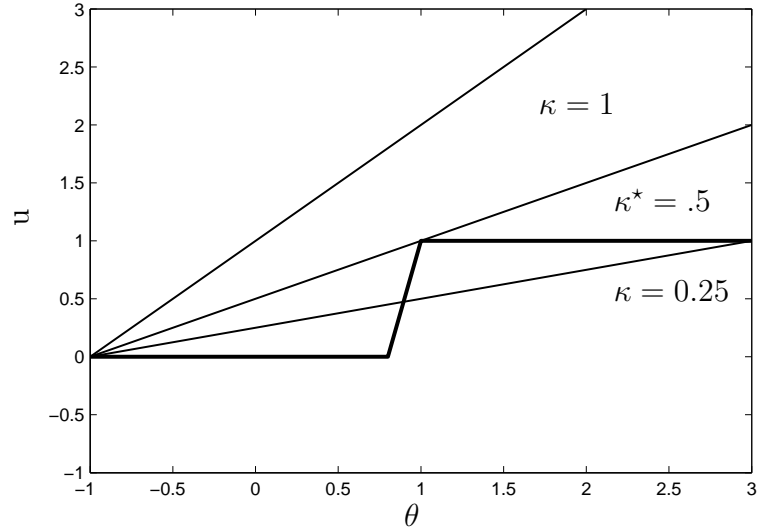
2.6   Traveling Wave Solution

The scaled Heaviside function is suited to one analytic approach when the interfacial resistance is zero. Recall the system of equations:

$$\theta_t = \theta_{xx} + u^2 + r(u_x)^2 + f(\theta)(1-u)^2 - \kappa(\theta - \theta_0)$$
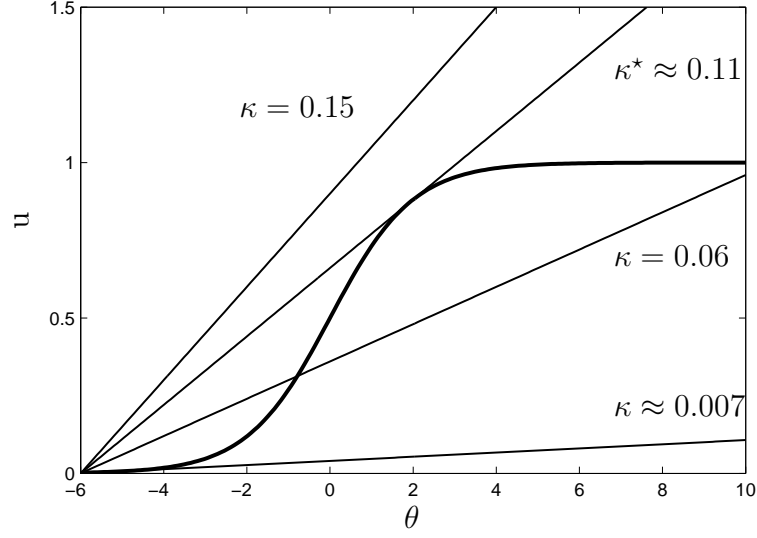
$$(ru_x)_x = u - f(\theta)(1-u)$$
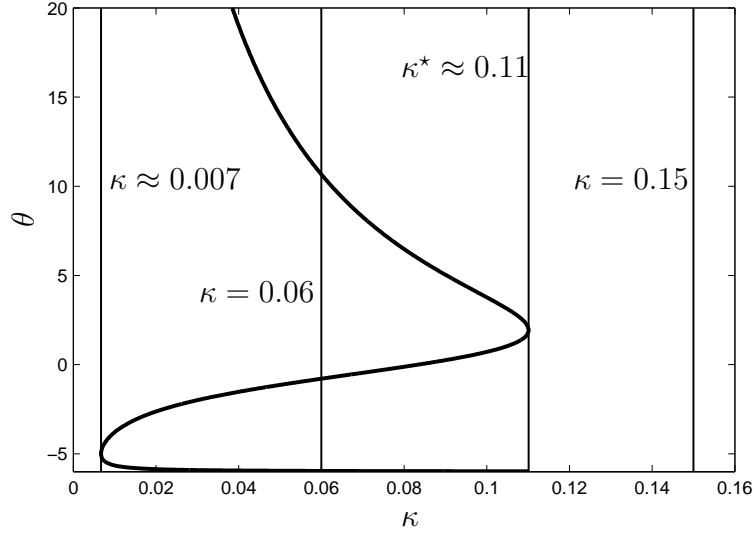
(a) Bistable solutions
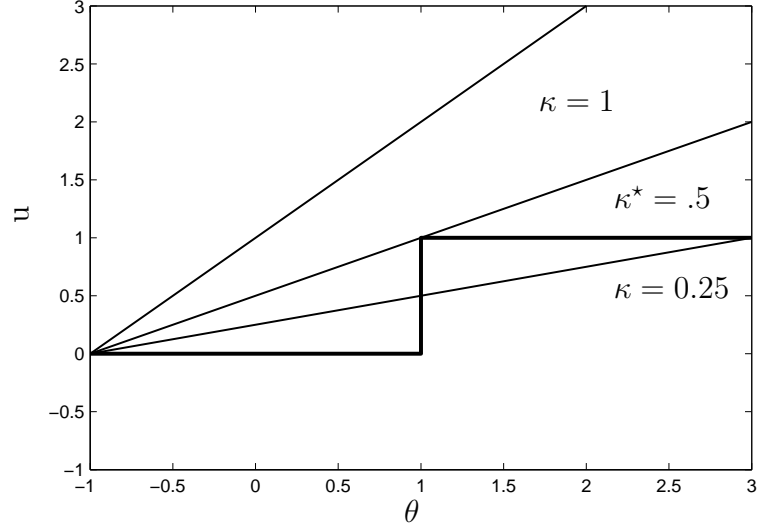
(b) Bistable solutions

Figure 8. The bistable solutions, indicated by the solutions of (8). For $\kappa > \kappa^\star$, there is only one stable solution, the low temperature solution. Note, the ramp function has been fixed for readability. In practice, the slope of the ramp is variable

19

(a) Bistable solutions

(b) Bistable solutions in the $\kappa\theta$-plane

Figure 9. **The bistable solutions, indicated by the solutions of** (8). **For** $\kappa > \kappa^\star$, **there is only one stable solution, the low temperature solution.**

Take the transition function $f(\theta) = \Gamma H(\theta)$, where $H(\theta)$ is the Heaviside function and $\Gamma \gg 1$ is a scaling parameter and let $r(x) = 0$. Then the system becomes:

$$\theta_t = \theta_{xx} + u^2 + f(\theta)(1-u)^2 - \kappa(\theta - \theta_0) \tag{9}$$

$$0 = u - f(\theta)(1-u). \tag{10}$$

The second equation can be solved for u

$$u = \frac{f(\theta)}{1 + f(\theta)} = \frac{\Gamma}{1 + \Gamma} H(\theta).$$

When $\kappa < \kappa_{\max}$, the solution has two stable equilibria

$$\theta(x) = \theta_0 \quad \text{and} \quad \theta(x) = \theta_{\max} = \theta_0 + \frac{1}{\kappa} \frac{\Gamma}{1 + \Gamma}.$$

Consider a the temperature distribution which consists of the two equilibrium solutions separated by an interface, specifically $\theta_{\max}$ on the left and θ_0 on the right as shown in Figure 10. The interface is not in equilibrium and hence it will evolve over time. A traveling wave solution merely translates without changing shape. Consider the traveling wave solution $\theta(x,t) = \theta(x - ct) = \theta(\xi)$ where c is the propagation speed of the interface. In this case

$$\theta_t = \theta_\xi \xi_t = -c\theta_\xi$$

and

$$\theta_x = \theta_\xi \xi_x = \theta_\xi \Rightarrow \theta_{xx} = \theta_{\xi\xi}.$$

For such a traveling wave solution (9) reduces to

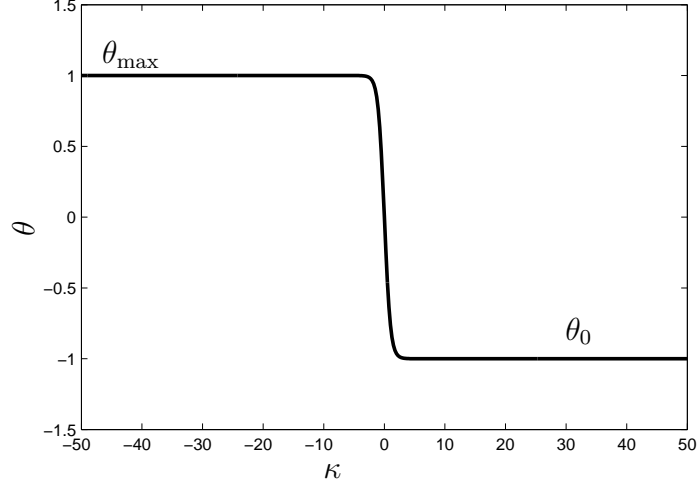$$-c\theta' = \theta'' + u^2 + f(\theta)(1-u)^2 - \kappa(\theta - \theta_0),$$

Figure 10. Equilibrium solutions $\theta_{\max}$ and θ_0 connected by a smooth interface. This interface is not in equilibrium so it will evolve over time.

or equivalently

$$\theta'' + c\theta' + u^2 + f(\theta)(1 - u)^2 - \kappa(\theta - \theta_0) = 0$$

an ordinary differential equation in ξ. This equation is the same as

$$\theta'' + c\theta' + M - \kappa(\theta - \theta_0) = 0, \qquad \text{for } \theta > 0 \qquad (11)$$

$$\theta'' + c\theta' - \kappa(\theta - \theta_0) = 0, \qquad \text{for } \theta < 0 \qquad (12)$$

with $M = \Gamma/(1 + \Gamma)$, because the transition function $f(\theta)$ is a scaled Heaviside function.

The homogeneous problem

$$\theta'' + c\theta' + \kappa\theta = 0$$

has the characteristic equation $r^2 + cr - \kappa = 0$ which has solutions

$$r_1 = \frac{-c + \sqrt{c^2 + 4\kappa}}{2} \quad \text{and} \quad r_2 = \frac{-c - \sqrt{c^2 + 4\kappa}}{2}.$$

22

Only r_1 will be considered, since r_2 would result in a negative speed for a front that is supposed to move to the right. The solutions to (11) and (12) are

$$\theta_-(x) = A_0 \exp(r_1 x) + B_0 \exp(r_2 x) + \frac{M}{\kappa} + \theta_0 \qquad \text{for } \theta > 1 \qquad (13)$$

$$\theta_+(x) = A_1 \exp(r_1 x) + B_1 \exp(r_2 x) + \theta_0 \qquad \text{for } \theta < 1. \qquad (14)$$

Where A_0, A_1, B_0 and B_1 are arbitrary constants. To ensure continuity and smoothness of the solution, the following boundary conditions and continuity conditions apply

1. $\lim\limits_{x \to \infty} \theta = \theta_0$

2. $\lim\limits_{x \to -\infty} \theta = \theta_{\max}$

3. $\theta_-(0) = 1 = \theta_+(0)$

4. $\theta'_-(0) = \theta'_+(0)$

Imposing boundary conditions 1 and 2 on (13) and (14) forces $B_0 = A_1 = 0$ and the solution becomes:

$$\theta_-(x) = A_0 \exp(r_1 x) + \frac{M}{\kappa} + \theta_0 \qquad \text{for } \theta > 1 \qquad (15)$$

$$\theta_+(x) = B_1 \exp(r_2 x) + \theta_0 \qquad \text{for } \theta < 1 \qquad (16)$$

Applying continuity conditions 3 to (15) and (16) yields

$$A_0 = 1 - \frac{M}{\kappa} - \theta_0 \qquad (17)$$

$$B_1 = 1 - \theta_0 \qquad (18)$$

Applying continuity condition 4 to the solutions and solving for the speed c gives

$$c = \left(\kappa \left(-4 + \frac{M}{M + \kappa \left(-1 + \theta_0 \right)} \right) - \frac{M}{-1 + \theta_0} \right)^{1/2}.$$

The traveling wave moves to the right $(c > 0)$ when

$$\kappa < \frac{M}{2 + 2|\theta_0|}$$

The speed c of the traveling wave can be be approximated by letting $M = 1$, and $\theta_0 = -1$. Figure 11 shows speed of the traveling wave c as a function of cooling κ. By extension a plateau solution consisting of three equilibrium solutions separated by two interfaces such as shown in Figure 16(a) on page 40 will grow if $\kappa < M/2 + 2|\theta_0|$ or shrink otherwise. This condition on κ appears to be necessary but not sufficient. Numerical results using the exponential and ramp transition functions require lower values of κ to guarantee a traveling wave solution in the case of no interfacial resistance.
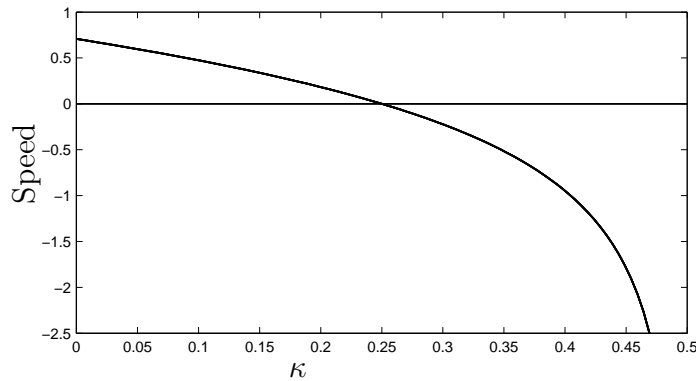

Figure 11. The speed of the traveling wave solution as a function of κ.

2.7 Dimensional Analysis

It is useful to develop an understanding of the importance of θ on the function $f(\theta)$. In general, whether an exponential term or a step function is used makes little difference in the types of solutions observed. The specifics of speed and regions may change, but the fundamental solution-types—heat gain or heat loss—remain the same. It is possible to observe the effect of scaling the coefficient of θ in the exponential term by introducing the coefficient α. This can be considered:

$$\theta_t = \theta_{xx} + u^2 + f(\alpha\theta)(1-u)^2 + r(u_x)^2 - \kappa(\theta - \theta_0)$$

$$(ru_x)_x = u - f(\alpha\theta)(1-u)$$

Then introduce ϕ in place of the term $\alpha\theta$:

$$\frac{1}{\alpha}\phi_t = \frac{1}{\alpha}\phi_{xx} + u^2 + f(\phi)(1-u)^2 + r(u_x)^2 - \kappa(\frac{1}{\alpha}\phi - \frac{1}{\alpha}\phi_0)$$

$$(ru_x)_x = u - f(\phi)(1-u)$$

Now, let $\tau = \alpha t$ and $\xi = x\sqrt{\alpha}$. The system of equations becomes:

$$\phi_\tau = \phi_{\xi\xi} + u^2 + f(\phi)(1-u)^2 + \alpha r(u_\xi)^2 - \frac{1}{\alpha}\kappa(\phi - \phi_0)$$

$$\alpha(ru_\xi)_\xi = u - f(\phi)(1-u)$$

This analysis shows that changing the transition function from $f(\theta)$ to $f(\alpha\theta)$ has the same effect as changing interfacial resistance from r to αr, changing the coefficient of cooling (inhibitor) from κ to κ/α, rescaling time from t to αt, and rescaling space from x to $\sqrt{\alpha}x$, while keeping $f(\theta)$ as the transition function. Hence, it is sufficient to examine $f(\theta)$ over a range of values for κ and r.

III. Numerical Method

3.1 Considerations

This section presents the development and details of the numerical method used to solve the system of equations

$$\theta_t = \theta_{xx} + u^2 + f(\theta)(1-u)^2 + r(u_x)^2 - \kappa(\theta - \theta_0) \tag{19}$$

$$(ru_x)_x = u - f(\theta)(1-u) \tag{20}$$

over a domain $x \in [-L, L]$ with either periodic or reflecting boundary conditions. While the wire can be considered infinitely long for the purposes of classical analysis, numerical analysis requires defined boundaries. For that reason, boundary conditions will be as follows. For periodic boundary conditions current and temperature will be allowed to flow across the boundaries

$$\theta(t, L) = \theta(t, -L), \quad \theta_x(t, L) = \theta_x(t, -L),$$

$$u(L) = u(-L), \quad \text{and} \quad u_x(L) = u_x(-L).$$

For reflecting boundary conditions current will be fixed at the boundaries to simulate current injection through the copper stabilizer and the boundaries will be thermally insulating

$$\theta_x(t, -L) = 0, \quad \theta_x(t, L) = 0, \quad u(-L) = 1, \quad \text{and} \quad u(L) = 1.$$

Reflecting boundary conditions are used to model a wire with terminals included. In the wire, the current will enter through the copper stabilizer before re-routing to

the superconductor. Reflecting boundary conditions require the specific adaptation

$$r(x) = \epsilon + r_0 \left(1 - e^{(\cos(x\pi/(2L))^2/c^2}\right)$$

to allow for the change in resistance necessary for current injection at the ends of the wire. The parameter c is the width parameter of the interface between resistance $r(x) \approx r_0$ to $r(x) \approx \epsilon$ at the boundaries. Without this modification, temperature builds at the boundaries as a result of the current crossing the interface between the superconductor and the stabilizer. Figure 12 on the next page shows the interfacial resistance along the length of the wire with reflecting boundary conditions. Notice the smooth transition from about $r_0 = 200$ in the bulk of the wire to almost zero resistance at the boundaries. Periodic boundary conditions represent a closed loop of wire. In this case, there is no change in resistivity so $r(x) = r_0$ throughout. Using reflecting or periodic boundary conditions results in essentially the same solution as long as the boundaries are avoided.

Initial conditions are given by

$$\theta(0, x) = \theta_0 + (a - \theta_0)e^{-x^2/2d^2} \tag{21}$$

where a is the temperature above critical temperature $\theta = 0$ and d is the width parameter. Equation (21) produces a Gaussian shape that models the distribution of initial heat.

This system presents two difficulties with regard to a numerical solution. The system is both stiff and nonlinear. The stiffness means there are differing time scales. That is, the solution exhibits both rapid changes and slow changes. An explicit method would involve a Courant–Friedrichs–Lewy (CFL) condition, $\Delta t \leq \Delta x^2/2$, which places sever restrictions on the step size for the purpose of stability. This
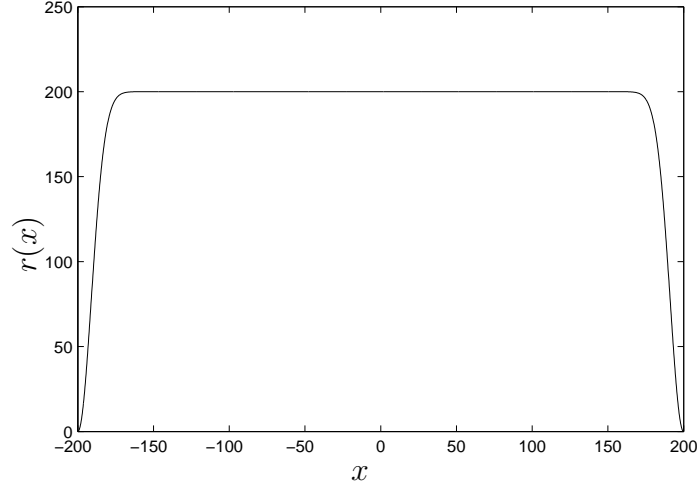
Figure 12. Interfacial resistance over the length of $[-L, L]$.

additional restriction would drive the time step to even smaller sizes, further extending the time to compute a solution. This means that an explicit method, which would generally be simpler to implement, would be impractical [11]. To achieve the desired level of accuracy, one would need to use very small step sizes making computation slow. An implicit method such as a Crank-Nicolson permits arbitrarily large step sizes because it is unconditionally stable with respect to the CFL condition. To maintain reasonable accuracy $\Delta t = O(\Delta x)$, which is not overly restrictive.

An explicit scheme is suitable for the non-stiff operators in the equations. An explicit method has the advantage of being simpler to implement than an implicit scheme, so it should be faster. The system is solved with a second-order implicit/explicit (IMEX) Adams-Bashforth/Crank-Nicolson method. The implicit portion takes care of the stiff linear terms, while the explicit portion addresses the nonlinear term(s). The IMEX Adams-Bashforth/Crank-Nicolson method is absolutely stable (A-stable). This means that it converges even for larger step sizes while maintaining second order accuracy [11]. For further details see [10] or [11].

28

3.2 Numerical Model

The domain is discretized using a uniform mesh $x_j = j\Delta x$ for $j = 0, 1, \ldots, N$ and a mesh size Δx. An IMEX Adams-Bashforth/Crank-Nicolson time marching scheme is used to solve (19) at each time step $t_n = n\Delta t$. Let Θ_j^n be the numerical approximation of the temperature $\theta(x_j, t_n)$ and U_j^n be the numerical approximation of current $u(x_j, t_n)$. The scheme is given by

$$\frac{\Theta_j^{n+1} - \Theta_j^n}{\Delta t} = \frac{1}{2}\left(H_j^{n+1} + H_j^n\right) + F_j^{n+1/2} \tag{22}$$

with

$$H_j^n = \frac{\Theta_{j+1}^n - 2\Theta_j^n + \Theta_{j-1}^n}{(\Delta x)^2} - \kappa\left(\Theta_j^n - \theta_0\right) \tag{23}$$

and

$$F_j^{n+1/2} = (U_j^{n+1/2})^2 + f(\Theta_j^{n+1/2})(1 - U_j^{n+1/2})^2 + r(x)_j\left(\frac{U_{j+1}^{n+1/2} - U_{j-1}^{n+1/2}}{2\Delta x}\right)^2 \tag{24}$$

for $j = 0, 2, \ldots, N$. The variable θ_0 is the non-dimensionalized ambient temperature. The current $U_j^{n+1/2}$ is computed by solving the numerical discretization of the Poisson equation (20)

$$\frac{r_{j+1/2}U_{j+1} - \left(r_{j+1/2} + r_{j-1/2}\right)U_j + r_{j-1/2}U_{j-1}}{(\Delta x)^2} = U_j - f(\Theta_j^{n+1/2})(1 - U_j) \tag{25}$$

where $r_{j+1/2} \equiv r(x_{j+1/2})$. When $r(x) \equiv r_0$ (25) simplifies to

$$r_0\frac{U_{j+1} - 2U_j + U_{j-1}}{(\Delta x)^2} = U_j - f(\Theta_j^{n+1/2})(1 - U_j) \tag{26}$$

for $j = 1, 2, \ldots, N-1$ with $\Theta_j^{n+1/2}$ approximated using the second-order extrapolation

$$\Theta_j^{n+1/2} = \tfrac{3}{2}\Theta_j^n - \tfrac{1}{2}\Theta_j^{n-1}.$$

The systems of equations (22) and (26) are not closed. Specifically, ghost points are necessary on the domain boundaries ($j = -1$ and $j = N + 1$). The ghost points are eliminated by the constraints given by the boundary conditions. To implement periodic boundary conditions (23) and (24) $j = 0$ and $j = N$ are replaced by

$$H_0^n = \frac{\Theta_1^n - 2\Theta_0^n + \Theta_N^n}{(\Delta x)^2} - \kappa\left(\Theta_0^n - \theta_0\right)$$

$$H_N^n = \frac{\Theta_0^n - 2\Theta_N^n + \Theta_{N-1}^n}{(\Delta x)^2} - \kappa\left(\Theta_N^n - \theta_0\right)$$

and

$$r_0\frac{U_1 - 2U_0 + U_N}{(\Delta x)^2} = U_0 - f(\Theta_0^{n+1/2})(1 - U_0)$$

$$r_0\frac{U_0 - 2U_N + U_{N-1}}{(\Delta x)^2} = U_N - f(\Theta_N^{n+1/2})(1 - U_N)$$

where r_0 is the interfacial resistance as previously defined. To implement reflecting boundary conditions, the following constraints are used to eliminate the ghost points at x_{-1} and x_{N+1}

$$\frac{\Theta_1^n - \Theta_{-1}^n}{2\Delta x} = 0$$

$$\frac{\Theta_{N+1}^n - \Theta_{N-1}^n}{2\Delta x} = 0$$

and using the second order approximation $u(x) \approx (u(x + \Delta x) + u(x - \Delta x))/2$

$$\frac{U_1 + U_{-1}}{2} = 1$$
$$\frac{U_{N+1} + U_{N-1}}{2} = 1.$$

By combining these constraints with (22) and (26)

$$H_0^n = \frac{2\Theta_1^n - 2\Theta_0^n}{(\Delta x)^2} - \kappa(\Theta_0^n - \theta_0)$$
$$H_N^n = \frac{2\Theta_{N-1}^n - 2\Theta_N^n}{(\Delta x)^2} - \kappa(\Theta_N^n - \theta_0)$$

and

$$r_0 \frac{2 - 2U_0}{(\Delta x)^2} = U_0 - f(\Theta_0^{n+1/2})(1 - U_0)$$
$$r_0 \frac{2 - 2U_N}{(\Delta x)^2} = U_N - f(\Theta_N^{n+1/2})(1 - U_N).$$

For the system of equations in which there is an exponential transition function, a centered difference method is used to solve (20) for u which is input into (19). Because the equation is linear with respect to u, the operator may be inverted using Gaussian elimination and the result is used in the time marching solution to (19). The system of equations in which there is a ramp as the transition function requires a fixed point iterative method to solve (20), because the ramp function is nonlinear with respect to u. A typical step size when exploring general forms of solutions has been $\Delta x = 0.25$. When computing specific values, such as front-speed, $\Delta x = 0.125$

Table 2. L1 error by step size

scale	1/2	1/4	1/8
error	0.00548	0.00127	0.00025

31

has been used. Table 2 on the preceding page shows L1 error relative to step size. L1 error is computed by

$$\text{error} = \sum_{i=1}^{N} |(\theta(x_i) - \Theta_i)|\Delta x$$

where $\theta(x_i)$ is the "exact" solution and Θ_i is the corresponding computed value for a given step size. The "exact" value is determined by solving the system with a small step size $\Delta x = 0.0625$. The ratios of the error terms confirm quadratic convergence of the method.

For reflecting boundary conditions the second derivative operator is a sparse tri-diagonal matrix. For periodic boundary conditions, the same operator is a sparse circulant matrix. Typical runtime for a simulation with $L = 200$, $t = 300$, 1600 mesh-points in space, 1200 mesh-points in time and reflecting boundary conditions will be about 22 seconds. Typical runtime for the same simulation modified for periodic boundary conditions is about 67 seconds. For reference purposes these times represent performance on a dual core 2GHZ processor.

IV. Taxonomy of Solutions

4.1 Map of Qualitative Regions

This chapter details the qualitative characteristics that define different solutions to the system

$$\theta_t = \theta_{xx} + u^2 + f(\theta)(1 - u)^2 + r(u_x)^2 - \kappa(\theta - \theta_0)$$

$$(r(u)_x)_x = u - f(\theta)(1 - u).$$

The solutions can be grouped into seven different families based on qualitative dynamics with six of these categories classified as failures. Recall that r_0 is interfacial resistance and κ is the cooling coefficient. When a wire is coiled for use in a magnet, its contact with the coolant is limited. This is different from a wire that is surrounded by coolant. For these reasons, r_0 and κ have been varied in the numerical model and the results studied. The initial question addressed the impact of interfacial resistance on speed of normal zone propagation. The results of this research, in addition to addressing that question, show solutions that are not so simple.

Figure 13(a) on the next page shows a map, in the $r_0\kappa$-plane, of the different regions for the system with an exponential transition function. Figure 13(b) shows a map for the system with a variable ramp as the transition function. The regions shown in the maps correspond to specific types of solutions. These maps correspond to solutions generated using specific initial conditions. In the case of the exponential transition function, the initial Gaussian shape was centered in space and had height and width parameters $a = d = 6$. In the map corresponding to the ramp transition function, these parameters were $a = 1.1$, $d = \sqrt{2}$. Changing these parameters will result in changes to these maps. The solutions have been categorized based on quan-
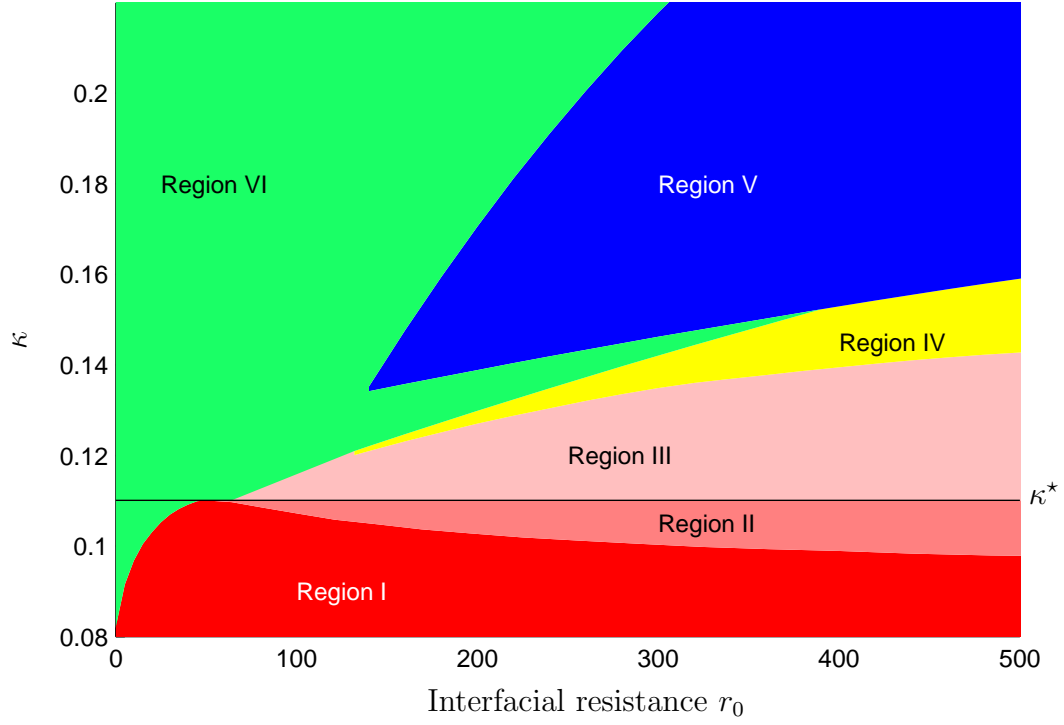
(a) Map of regions with $\exp(\theta)$ transition function
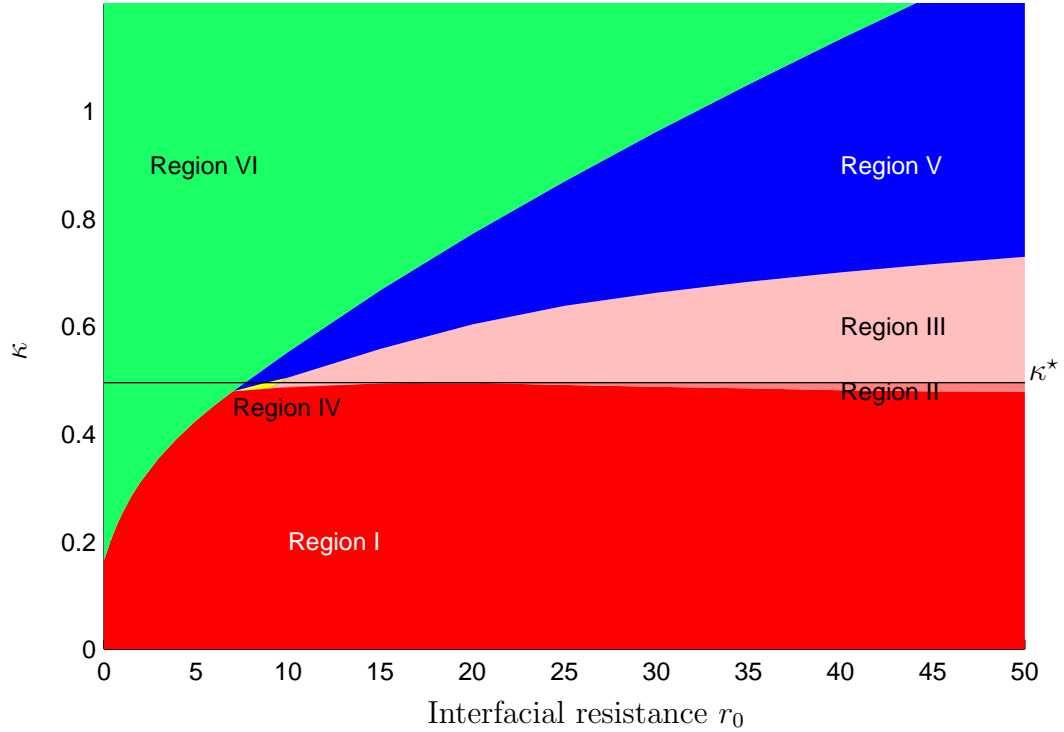
(b) Map of regions with ramp transition function

Figure 13. Maps of qualitative regions in the $r_0\kappa$ phase-plane. In figure (a) initial conditions, see equation (21), are $a = d = 6$; $\kappa^\star \approx 0.1101$. In figure (b) initial conditions are $a = 1.1$, $d = \sqrt{2}$; $\kappa^\star = 0.495$.

34

titative as well as qualitative differences. The quantitative descriptors are listed in Section 4.1.1 .

The regions can be described as follows. The Adiabatic Region, not shown in Figure 13(a), corresponds to the *adiabatic* case where heat increases, but $\kappa = 0$ so there is no cooling. In this region θ increases unbounded and the profile of θ resembles a triangle expanding over time. Region I is also characterized by an increase in temperature, but there is an upper bound for θ. A solution in this region resembles a horizontally expanding plateau similar to the traveling wave solution detailed in section 2.6. Solutions in Region II are also described by traveling waves but as an upper bound for θ, they have small peaks that form at the trailing edges of the moving fronts. Solutions in all three of these regions display increasing temperature with the maximum value of θ in Regions I and II consistent with analysis of constant equilibrium solutions in Chapter 2. The solutions in Region III can be described as *dissipative solitons* [1]. Dissipative solitons differ from classical solitons in that their shapes are not necessarily constant, and their rate of motion is not determined by their initial conditions. Instead they can pulsate and their rate of motion is characterized by system parameters. While classical solitons may interact, in dissipative solitons interaction is limited to the edges of their tails [1]. In Region III, the solitons will be generated continuously on an infinite domain and spread along the length of the wire. In Region IV, the initial Gaussian shape splits into two solitons that will begin pulsating as they move away from each other until they encounter a change in interfacial resistance or another soliton. At that point they will be repelled and move back in the opposite direction. In Region V, the initial Gaussian undergoes a change in shape and size, but does not move. The resulting distribution is a stationary, non-pulsating soliton. In Region VI, the initial Gaussian dissipates completely and all heat is absorbed by the cooling forces.

The map for the regions for solutions of the system with ramp transition function is qualitatively similar to the map of regions for the system with exponential transition. The Adiabatic Region and Regions I and II contain solutions that can be described as having continuously increasing heat. In each case, the boundary locations are determined by initial conditions. For example, increasing the width parameter d in the initial Gaussian shape means that it is necessary to increase interfacial resistance in order to observe solutions in Region V. This is reasonable because in equation (1) the gradient of the current u_x is multiplied by r interfacial resistance, and therefore $r(u_x)^2$ can held at a fixed value for appropriate values of u_x and r.

For a fixed value of interfacial resistance, varying the cooling coefficient κ will change the types of solutions that are observed. For example, if $r_0 = 20$ then $\kappa = 0.103$ will produce a solution in Region I. Increasing cooling so that $\kappa = 0.104$ produces a solution in Region VI. This qualitative change in solutions is a *bifurcation*. While the location of bifurcation points is dependent on initial conditions, the characteristics of the regions are not. In other words the solutions to this system are robust with respect to background noise or subtle changes to initial conditions. $\theta_{\max}$, front speed and the behavior of solitons are determined by the system conditions, κ, $r(x)$ and $\exp(\theta)$, rather than initial conditions. This differs from conservative systems where the speed of a soliton may be altered by adding noise or changing its initial conditions [1].

As mentioned in Section 2.4 the solutions to the system of equations have two stable equilibrium, normal conductivity corresponding to high (above critical) temperature and superconductivity corresponding to low temperature. In the first case, heat is generated and there is not enough cooling capacity to adequately disperse it. After a short time as heat builds, this normal zone will spread or propagate at a constant rate. In the latter case, heat is generated, but it is quickly dispersed. This is the case both when there is a high cooling coefficient $\kappa > \kappa^\star$ with low interfacial

resistance, and when the shape of the initial Gaussian does not have a large enough gradient u_x or the initial Gaussian is not high enough $a < |\theta_0|$.

Figure 14 on the following page shows the initial Gaussian shape produced by (21), with $a = d = 6$, used to model initial temperature in the majority of this research. These are the initial conditions used to generate Figure 13(a) on page 34. Modifying the initial heat distribution can, in some cases, change the solution observed. This will be addressed in the following sections.

4.1.1 Quantitative Descriptors.

Where appropriate, a few quantities are used to describe the solutions and characterize the regions. *Maximum temperature*, referred to as $\max(\theta)$, is defined as

$$\max_{x \in [-L,L]} (\theta(t))$$

and quantifies the maximum temperature of the solution in the domain. *Total heat* is defined as

$$\int_{-L}^{L} \theta(x, t) \, dx$$

and quantifies the total temperature above θ_0. *Total variation* is defined as

$$\mathrm{TV}(t) = \int_{-L}^{L} |\frac{\mathrm{d}}{\mathrm{d}x} \theta(x, t)| \, dx.$$

Total variation quantifies the total change in temperature in the region. For example, for a constant function, say $f(x) = 5$, total variation would be zero. For $f(x) = \sin(x)$ over the interval $[-\pi, \pi]$, total variation would be two.
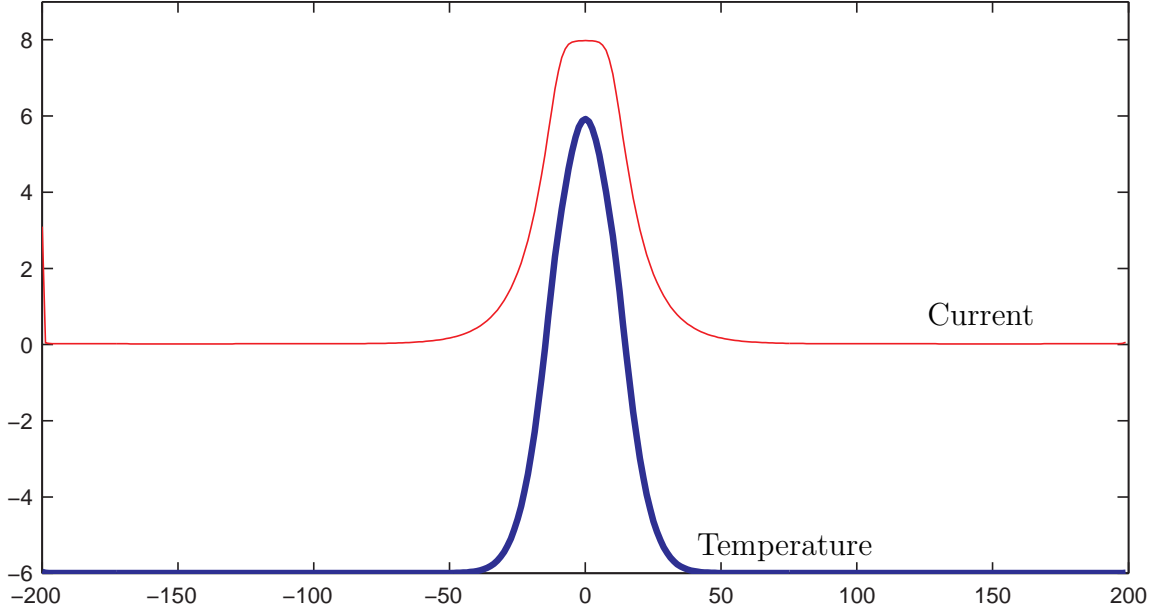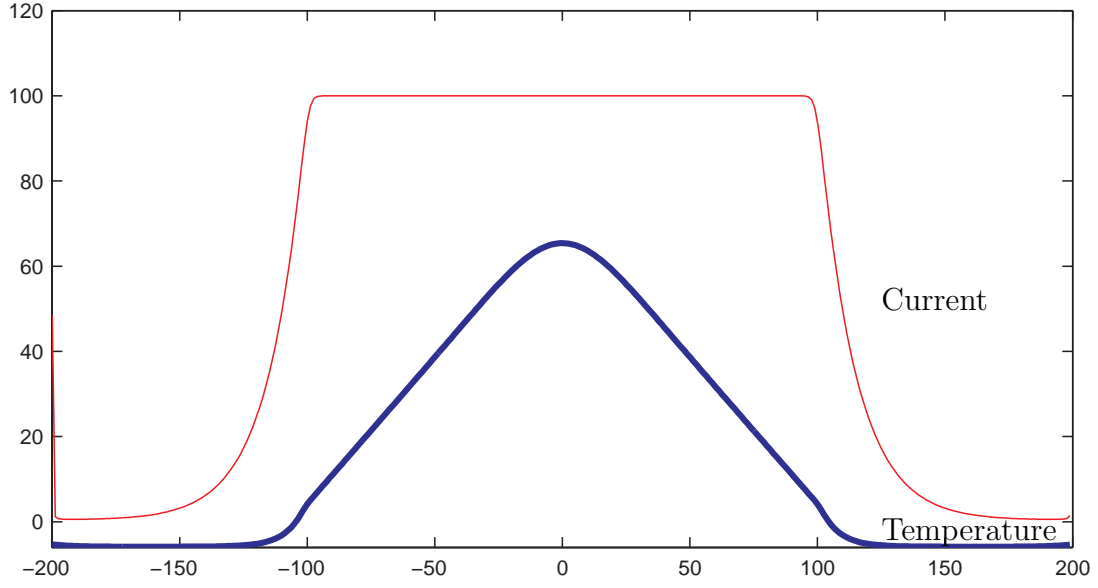
Figure 14. **A cross-section of the initial dimensionless temperature and ratio of current, showing the perturbation of each. The ratio of current $u \in [0,1]$ is not to scale in this image.**

4.2 Adiabatic

The Adiabatic case is the set of $\kappa = 0$ and r_0 for which a temperature profile $\theta(x,t)$—starting with the Gaussian distribution—will grow unbounded. As the normal zone propagates along the length of the wire, the temperature will climb until current is shut off or the wire is destroyed. Figure 15(a) on the following page shows the distribution of θ for $\kappa = 0$ and $r_0 = 200$ at time $t = 62.5$. The distribution of θ resembles a triangle with height θ_{max} and base $2x_0$, where x_0 is the point where $\theta = 0$. In the Adiabatic case, total variation is increasing, as are total heat and $\max(\theta)$.

4.3 Region I

Region I is the set of κ and r_0 for which a temperature profile $\theta(x,t)$—starting with the Gaussian distribution—will grow, but there is an upper bound to θ. The solution in this region resembles a monotonic expanding front, or a traveling wave. As
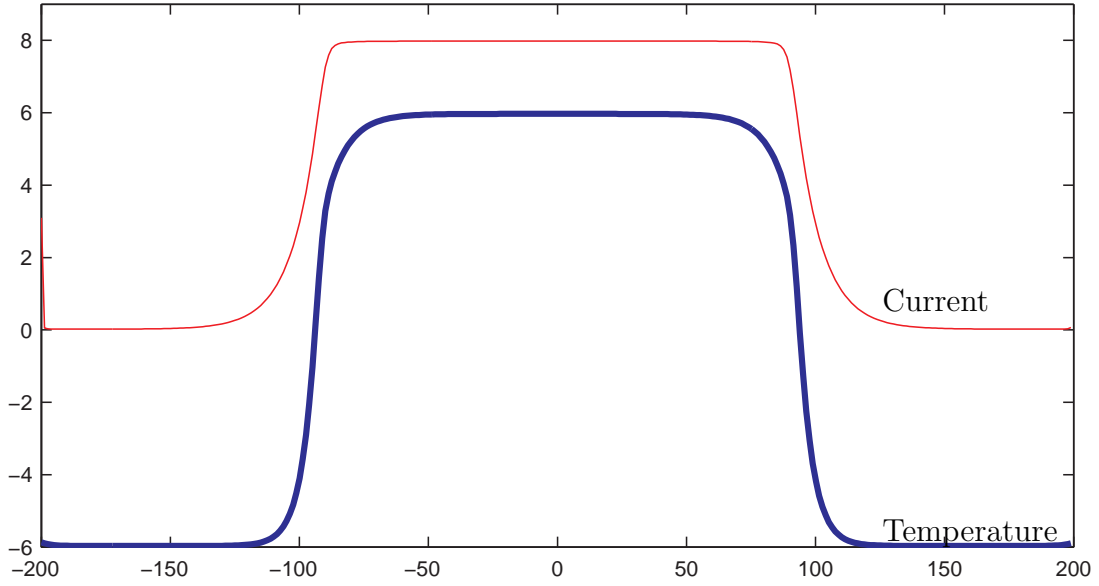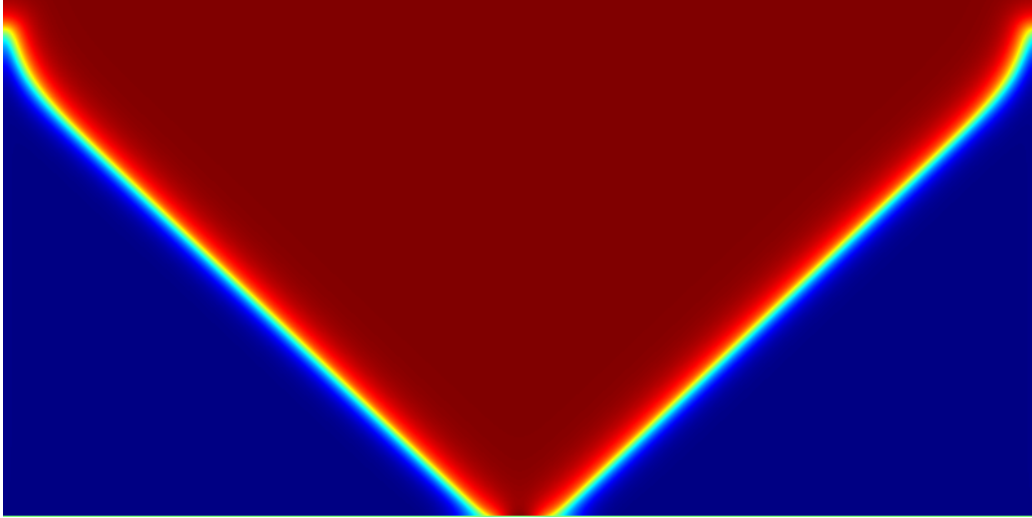
(a) Current and Temperature Distribution
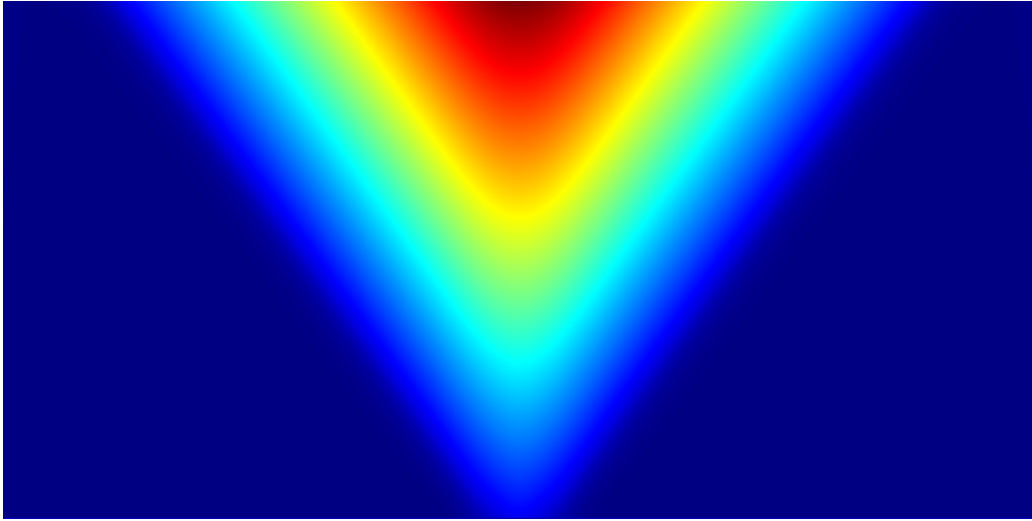
(b) Evolution

Figure 15. (a) **A snapshot at time** $t = 62.5$ **of dimensionless temperature and ratio of current. The ratio of current** $u \in [0, 1]$ **is not to scale in this image. (b) The evolution of the solution in time, x-axes show distance** $L = 200$, **y-axes show total time** $t = 100$, $\Delta t = \Delta x = 0.25$, **red indicates high temperature, blue indicates low temperature. In black and white images, the area above/inside each 'V' is higher temperature than the rest of the region. In the adiabatic case, the wave front is not as pronounced as it is in Regions I and II.**

(a) Current and Temperature Distribution

(b) Evolution

Figure 16. (a) **A snapshot at time** $t = 150$ **of dimensionless temperature and ratio of current for** $r_0 = 200$ **and** $\kappa = 0.08333$. **The ratio of current** $u \in [0, 1]$, **is not to scale in this image.** (b) **The evolution of the solution in time, x-axes show distance** $L = 200$, **y-axes show total time** $t = 400$, $\Delta t = \Delta x = 0.25$, **where red indicates high temperature and blue indicates low temperature. In black and white images the area inside the 'V' is the high temperature region.**

40

the total temperature θ increases, the top of the curve will flatten out. Figure 16(a) on the previous page shows the distribution of θ for $\kappa = 0.08333$ and $r_0 = 100$ at time $t = 150$. This solution corresponds to heat build up and the conversion to normal mode with a continuous normal zone and normal zone propagation. While there is normal zone propagation in these solutions, the temperature remains bounded and should grow enough to damage the wire. It occurs when κ is too weak to inhibit quench. For solutions in this Region, total variation is roughly constant, while total heat is increasing and $\max(\theta)$ approaches $\theta_{\max}$ described in Chapter 2.

4.3.1   Front Speed.

The speed of the traveling wave can be found numerically by tracking the position at which $\theta(x, t) = 0$ and computing its speed. Because $\theta(x, t) = 0$ lies between mesh-points, linear interpolation is used to approximate its location. Some care is taken to avoid approaching the boundary. Figure 17(a) on the following page shows front-speed as a function of κ and $\sqrt{r_0}$. It illustrates the fact that as r_0 increases, so does the speed of the traveling wave, as roughly the $\sqrt{r_0}$, for values of κ as low as the adiabatic case. After computing front speed, linear regression is used to determine the speed as a function of κ and r_0. In the system with exponential transition function, the speed S can be expressed as $S(\kappa, r_0) = 1.26 - 16.3\kappa + .055r_0$.

While it is useful to find the front-speed, it is more important to know what that speed is relative to the rate of change of $\max(\theta)$. Recall that in the adiabatic or near-adiabatic case, $\max(\theta)$ may reach the point of permanent damage before a normal zone can be detected. Figure 17(b) shows the ratio of $\max(\theta)$ to x_0 as a function of $\sqrt{r_0}$.

(a) Front-speed

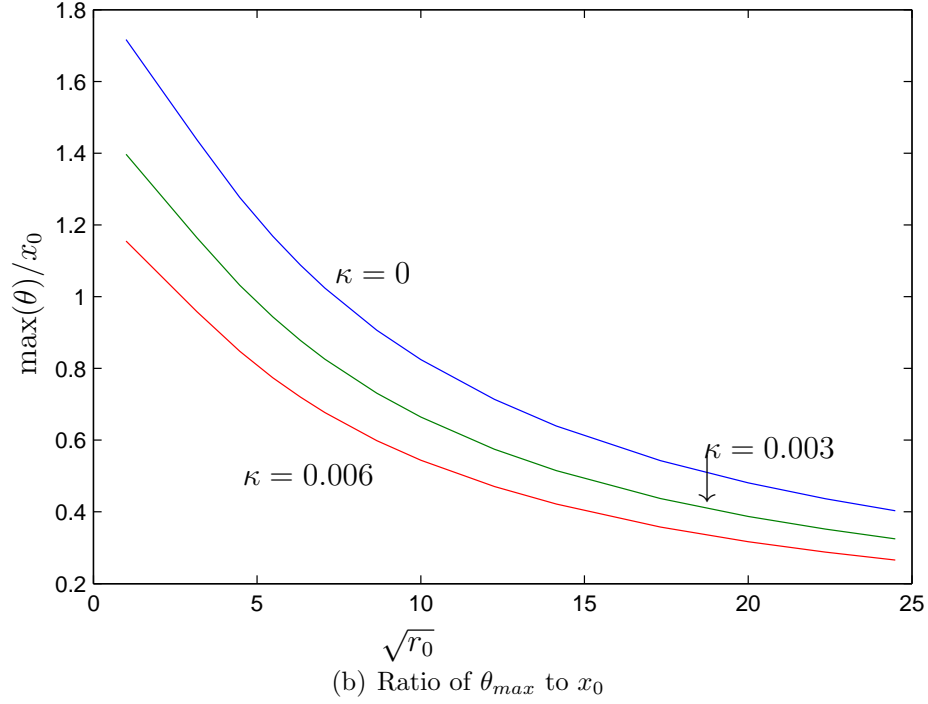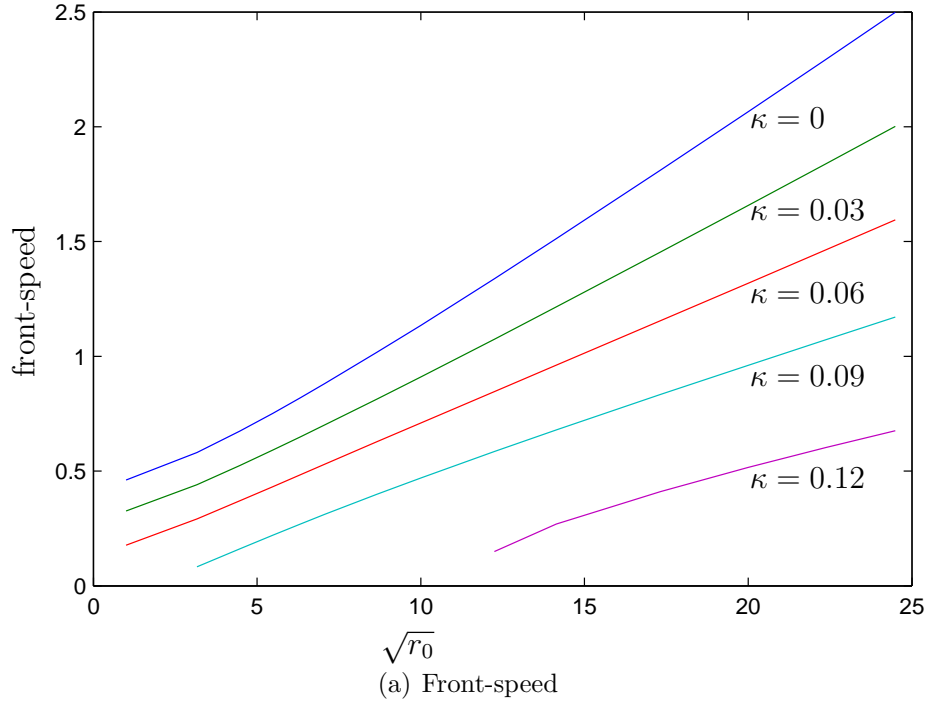

(b) Ratio of θ_{max} to x_0

Figure 17. (a) Front-speed as a function of $\sqrt{r_0}$ for parameter $0 \leq \kappa \leq 0.12$. Note that even though values of κ are uniformly spaced, the change of front-speed is not uniform. $\kappa = 0.12$ is the only value that is above the analytically predicted $\kappa^\star \approx 0.1101$. (b) The ratio of $\max(\theta)$ to x_0 as a function of $\sqrt{r_0}$ for parameter $0 \leq \kappa \leq 0.006$. Note that κ is restricted to the adiabatic or nearly adiabatic case.

42
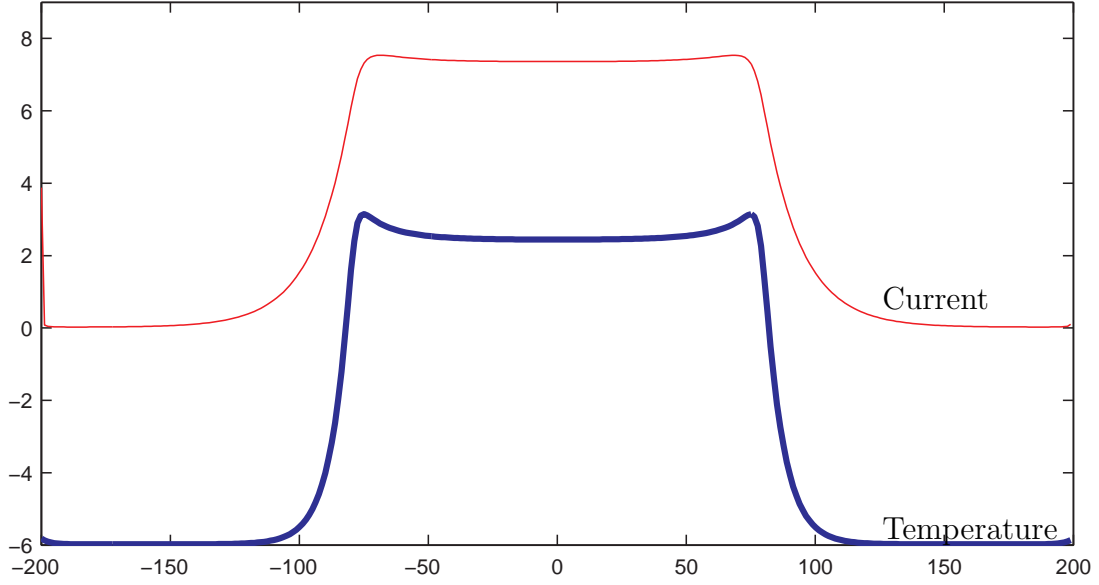
(a) Current and Temperature Distribution
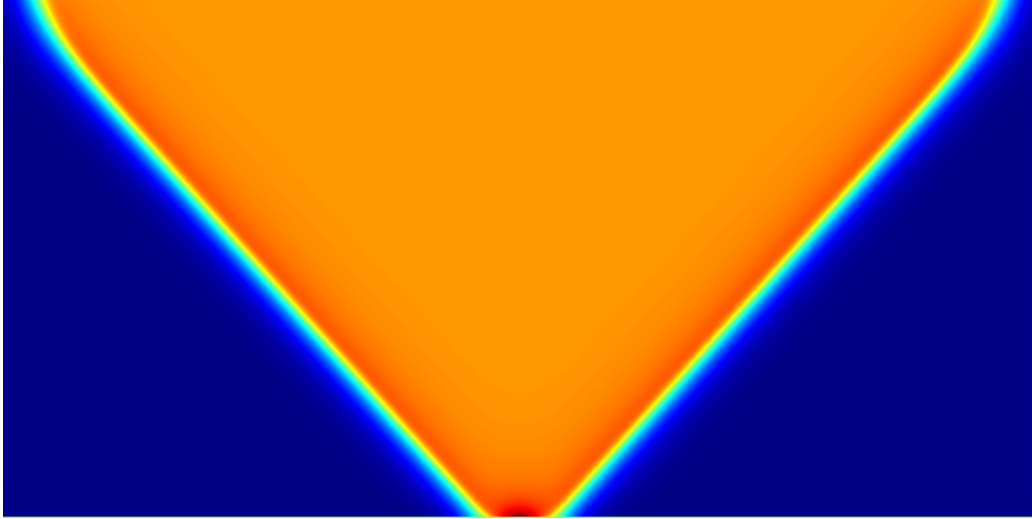
(b) Evolution

Figure 18. (a) **A snapshot at time** $t = 150$ **of dimensionless temperature and ratio of current for** $r_0 = 200$ **and** $\kappa = 0.109$. **The ratio of current** $u \in [0, 1]$ **is not to scale in this image.** (b) **The evolution of the solution in time, x-axes show distance** $L = 200$, **y-axes show total time** $t = 400$, $\Delta t = \Delta x = 0.25$, **red indicates high temperature, blue indicates low temperature. In black and white images, the area above/inside the 'V' is the high temperature region. In this region, the temperature inside the 'V' is actually lower than the temperature of the 'V'.**

43

4.4 Region II

Region II is the set of κ and r_0 for which a temperature profile $\theta(x,t)$—starting with the Gaussian distribution—will expand as a traveling wave, in a manner similar to Region I, except for small peaks that form at the trailing edge of the moving fronts of the solutions. Figure 18(a) on the previous page shows the distribution of θ for $\kappa = 0.109$ and $r_0 = 200$ at time $t = 150$. While the front in Region I is monotonic in space, Region II presents a non-monotonic expanding front with a local maximum at each edge of the plateau. Temperature θ for the plateau region is consistent with values predicted by (8). The height of the local maximum, θ_{peak}, has been computed numerically. Figure 19 on the following page shows the relation between this height, relative to the predicted θ_{max}, and r_0 for several values of κ. The peaks are caused by increased cooling coupled with high interfacial resistance. The increase in cooling makes the gradient of the front higher increasing the heating contributed by the $r(u_x)^2$ term. This region is quantitatively similar to Region I; total variation and $\max(\theta)$ are roughly constant with total heat increasing as the normal zone propagates. Like Region I, the failures described by the solutions are not likely to lead to damage or destruction of the wire.

4.5 Region III

Region III is the set of κ and r_0 for which a temperature profile $\theta(x,t)$—starting with the Gaussian distribution—expands outward with variable θ between the fronts. The front-speed can be determined as for previous Regions. Figure 17(a) on page 42 includes computed speed for κ and r_0 representative of this Region.

The solution consists of continuously generated solitons which will move unless they are kept stationary by their neighbors and boundary conditions. Since this is a non-conservative system these solitons are referred to as *dissipative solitons* [1]. Dis-
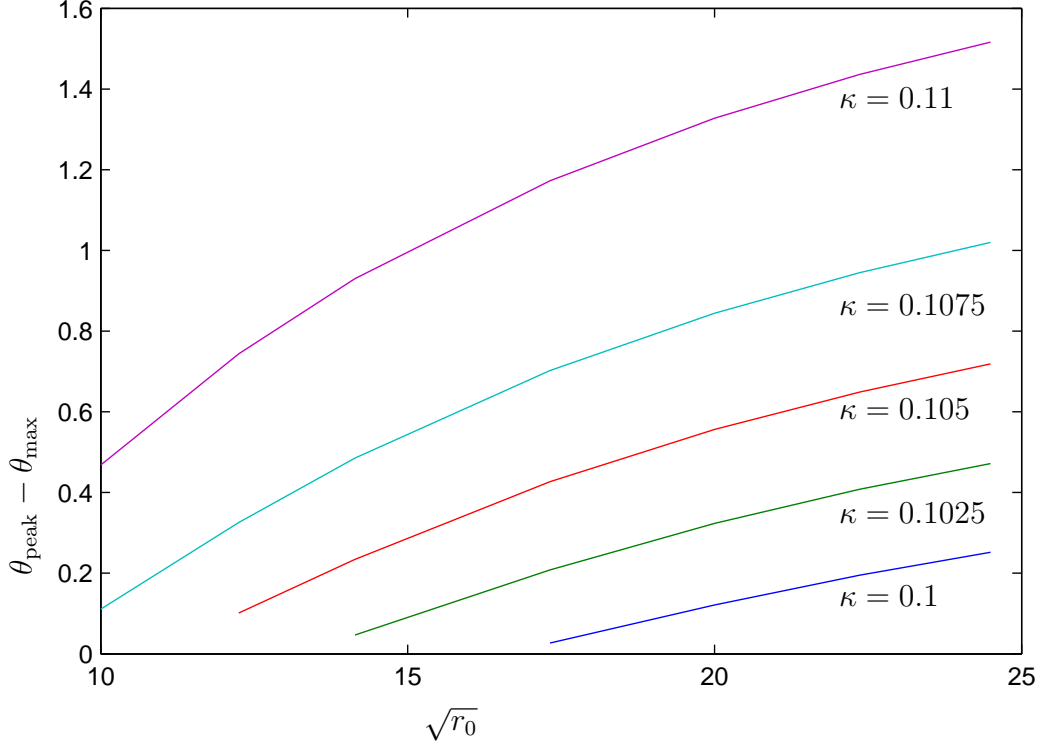
Figure 19. Overshoot θ_{peak} minus predicted maximum θ_{max} as a function of $\sqrt{r_0}$ for parameter κ in Region II

sipative structures, have been observed in various biological, chemical, and physical settings such as gas-discharge systems, nonlinear optical systems, and nerve pulses. They have also been described by a variety of reaction-diffusion systems in one to three dimensions [1, 2, 4, 13]. In this Region normal zones are created which subsequently move but do not necessarily expand or dissipate. Figure 20(a) on the following page shows a typical profile of θ for $\kappa = 0.115$ and $r_0 = 200$ at time $t = 150$.

For some values of κ, after the initial propagation of heat the solitons will be generated until they have filled the available space and then they will stop moving. Figure 21(a) on page 48 shows a solution when $\kappa = 0.1109$, $r_0 = 300$, and $L = 200$. Notice that after the solution reaches the boundaries, there is no further change in the distribution. In other cases, solitons will develop but will continue pulsating as shown in Figure 21(b), where $\kappa = 0.1115$, $r_0 = 300$, and $L = 200$. In this case, the change in κ has caused the width of the solitons to decrease and they will continue
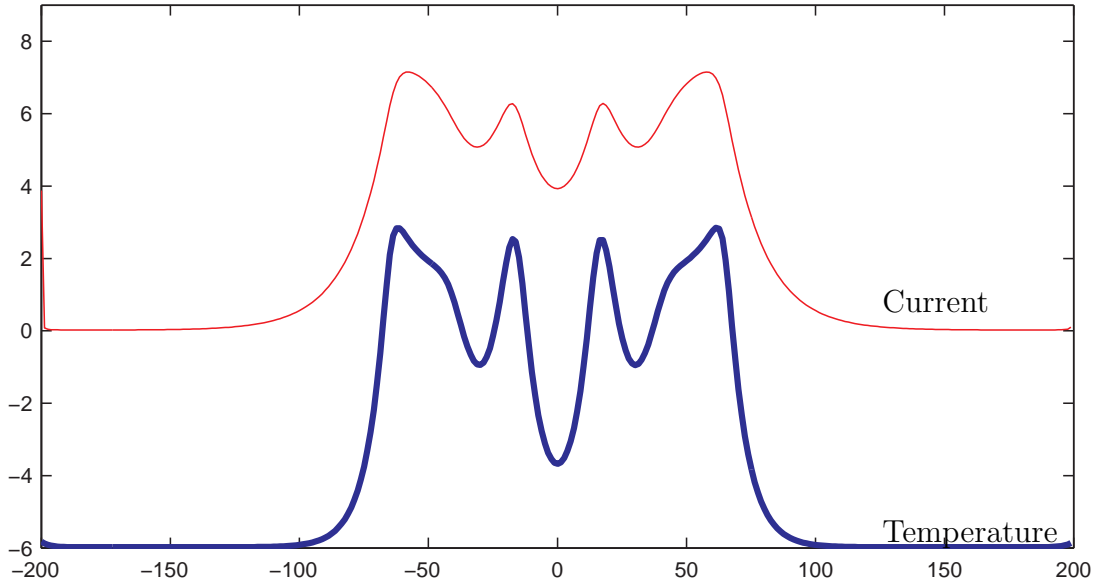
(a) Current and Temperature Distribution
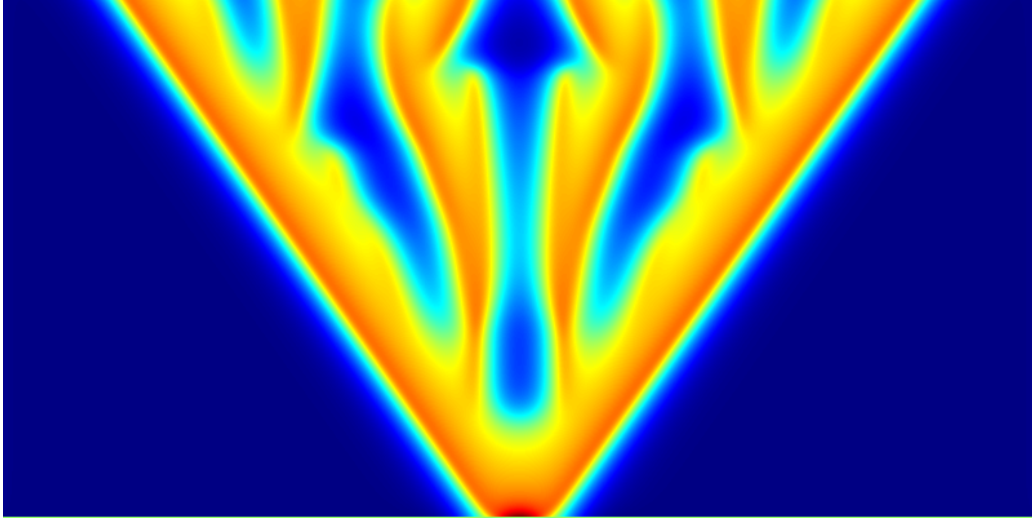
(b) Evolution

Figure 20. (a) **A snapshot at time** $t = 150$ **of dimensionless temperature and ratio of current. The ratio of current** $u \in [0, 1]$ **is not to scale in this image.** (b) **The evolution of the solution in time, x-axes show distance** $L = 200$, **y-axes show total time** $t = 400$, $\Delta t = \Delta x = 0.25$, **red indicates high temperature, blue indicates low temperature. In black and white images, the area above/inside the 'V' is the high temperature region.**

46

attempting to *bud* or generate new solitons. There is insufficient space for additional solitons, so the solution develops a pattern in time. In some of these instances, a pattern of generation and annihilation develops that does not subside over time as shown in Figure 22(b) on page 49, where κ =0.115, r_0 = 100, and L = 210. In all cases, solitons will generate and organize into a pattern. The pattern will be stationary if length L is an integer multiple of the width of a soliton. This pattern is demonstrated for several domain sizes in Figures 22(a), 22(b), 22(c), and 22(d) on page 49. As L increases, the qualitative nature of the solution, after reaching the boundaries, changes. Before the solitons reach the boundaries, all four solutions are the same. This suggests that in the absence of boundaries, in a very long wire for example, the solitons will continue moving and budding.

The nature of the solutions in this region is influenced by κ, r_0, and size of the spacial domain L. In general, the solutions are similar to that shown in Figures 21(a) and 21(b), but solutions close to the boundary of Region IV or Region VI—high κ— will develop fewer solitons, and in the neighborhood of a bifurcation it is possible to observe symmetry breaking behavior.

In Region III, max(θ) is not predicted by analysis in Chapter 2 and is not high enough to cause damage to the wire. Solutions in Region III display a bounded-oscillating max(θ), increasing total variation until boundary effects restrict further increase and an increase in total heat.

4.5.1 Ramp Transition Function.

Unlike the solutions for the exponential transition function, the numerical solutions for the ramp transition function are sensitive to mesh-size away from bifurcation points, see Figures 23(a), 23(b), and 23(c) on page 51. The solutions shown share identical values of κ, r_0, and L. The mesh-size decreases from .25 to .0625. In the

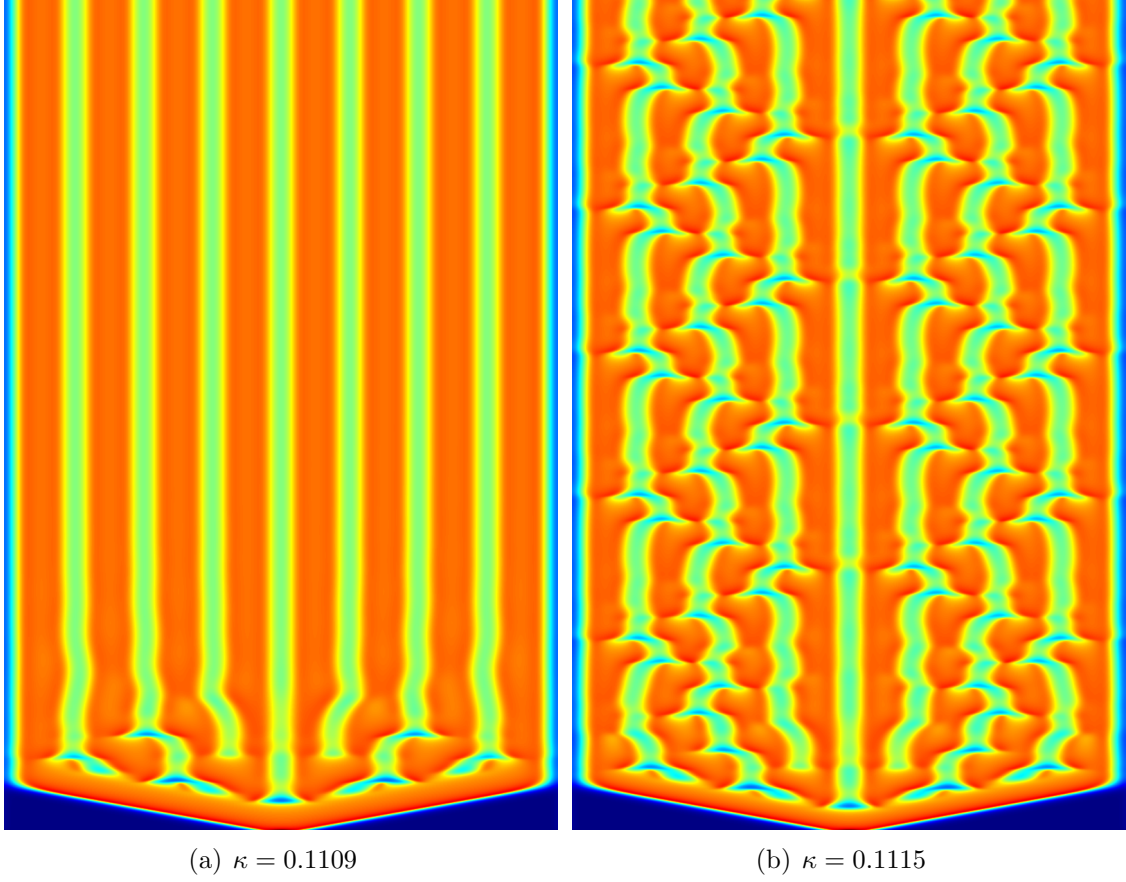(a) $\kappa = 0.1109$ (b) $\kappa = 0.1115$

Figure 21. Effect of varying the cooling coefficient κ on the evolution of solutions over time, x-axes show length when $L = 200$, y-axes show total time $t = 6000$, $\Delta t = \Delta x = 0.25$. (a) A stationary and non-pulsating solution, $r_0 = 300$, $\kappa = 0.1109$. (b) A pulsating solution, $r_0 = 300$, $\kappa = 0.1115$.
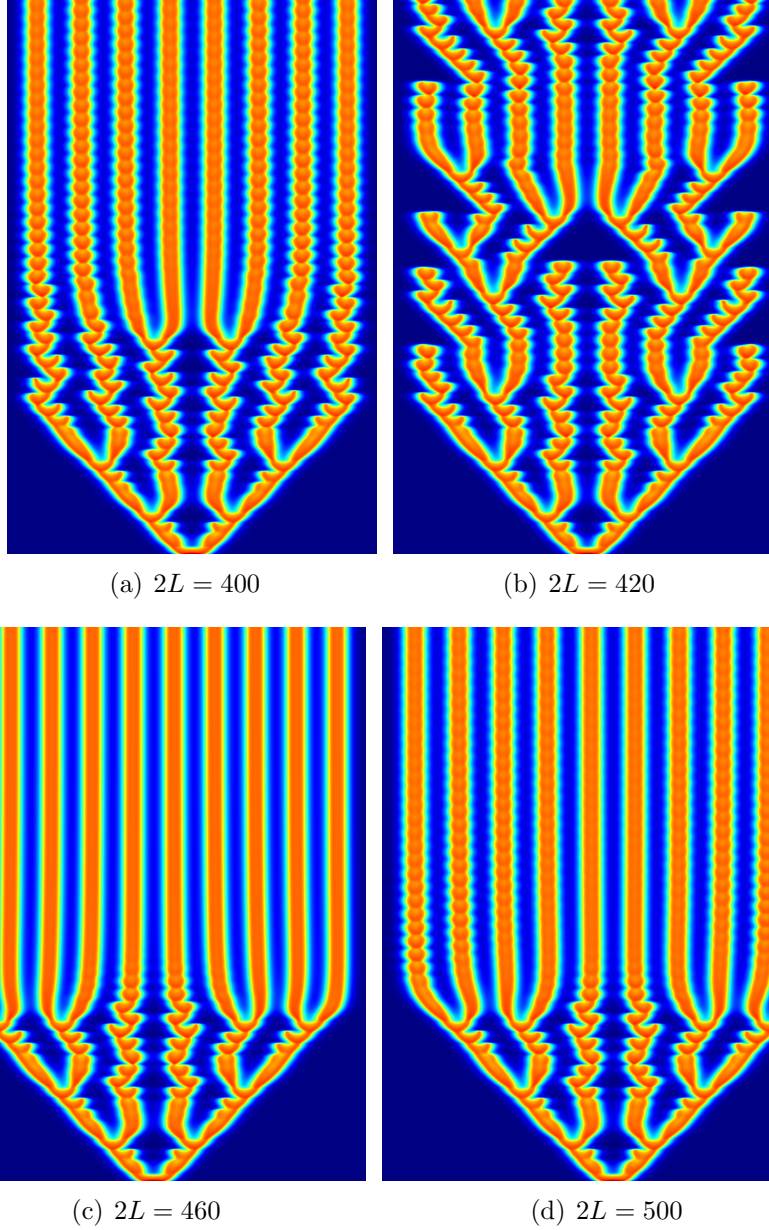
(a) $2L = 400$ (b) $2L = 420$

(c) $2L = 460$ (d) $2L = 500$

Figure 22. **Effect of varying the length of domain on the evolution of solutions over time, x-axes show length $2L$ ranging from 400 to 500, y-axes show total time $t = 6000$, $\Delta t = \Delta x = 0.25$. All images produced with $r_0 = 100, \kappa = 0.115$. (a) A stationary, pulsating system of solitons. (b) A cycle of creation and annihilation of solitons. (c) A stationary, non-pulsating system of solitons. (d) A stationary, pulsating system of solitons.**

49

case of the ramp transition function, the difference in computed front-speed due to mesh-size has an impact on the behavior of the solitons in this region. Notice that, unlike the solutions shown previously, the difference in behavior occurs well before boundary effects have an impact on the solution.

4.6 Region IV

Region IV is the set of κ and r_0 for which a temperature profile $\theta(x,t)$—starting with the Gaussian distribution—will evolve into traveling solitons. The solitons may display pulsating behavior that looks like a galloping motion as seen in Figure 25(a) for parameters $\kappa = 0.14$ and $r_0 = 350$. This region, like Region III, does not exist for low interfacial resistance. Figure 24(a) on page 52 shows the distribution of θ for $\kappa = 0.14$ and $r_0 = 350$ at time $t = 150$. This is similar to the budding observed in Region III, and the movement is similar as well. Each soliton will start to bud and split into two solitons but the cooling force is strong enough to prevent a complete split. Instead, the soliton will swell, developing dual peaks. One peak will die off while the other will continue in the direction of the original soliton. This budding is suppressed for large values of r_0, and for these values there is only initial movement to an equilibrium position as shown in figure 25(b) where $\kappa = 0.19$ and $r_0 = 3500$. In the pulsating case, the solitons move in one direction until they encounter another soliton at which point both will be repelled and proceed in the opposite direction. This behavior is unlike the behavior of solitons in a conservative system. Solitons in a conservative system may interact in a manner that includes a large soliton overtaking a smaller soliton and a resulting change in mass and speed. In the case of dissipative solitons, interaction is typically limited to the tails or edges of the solitons [1]. As in Region III, symmetry breaking can occur in the bifurcation regions. In considering the interactions of these solitons, it is not unreasonable to treat them as particles, or
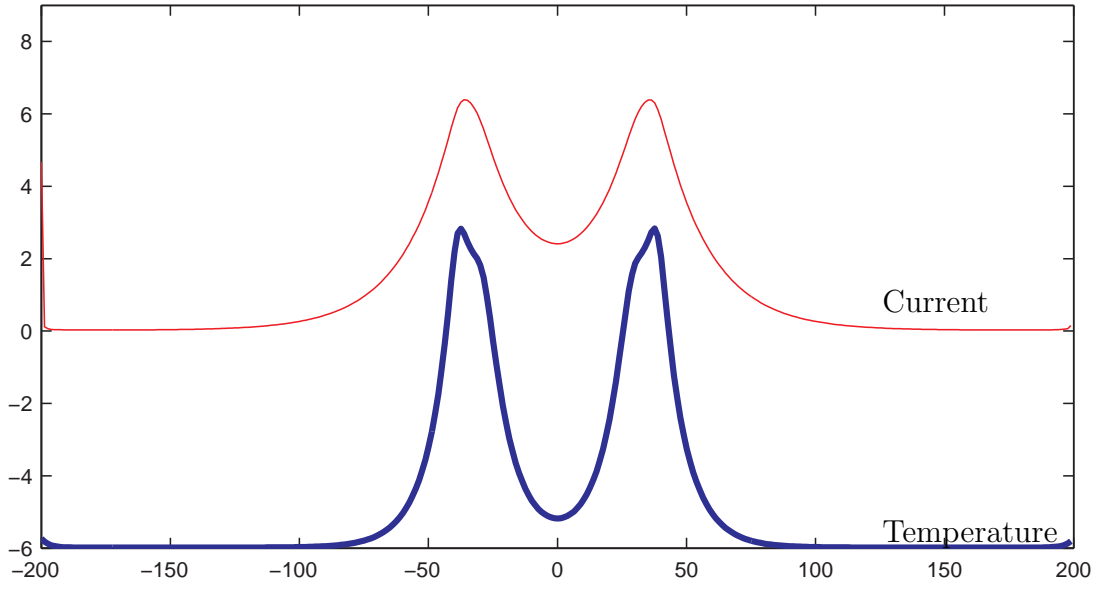
50
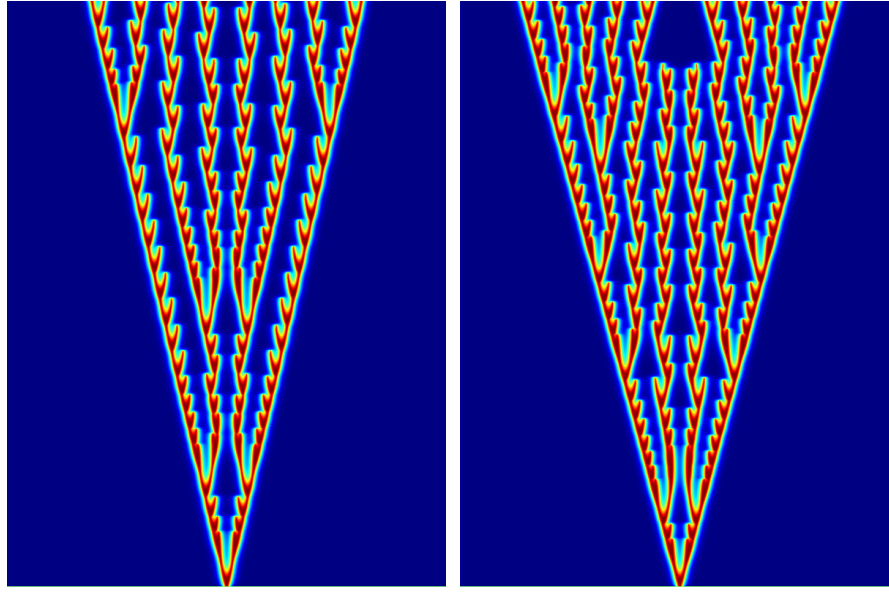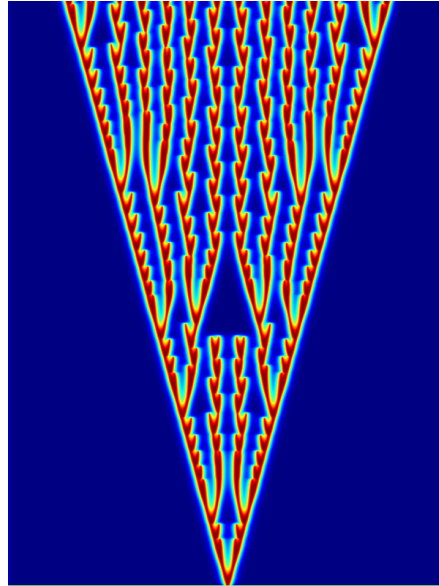
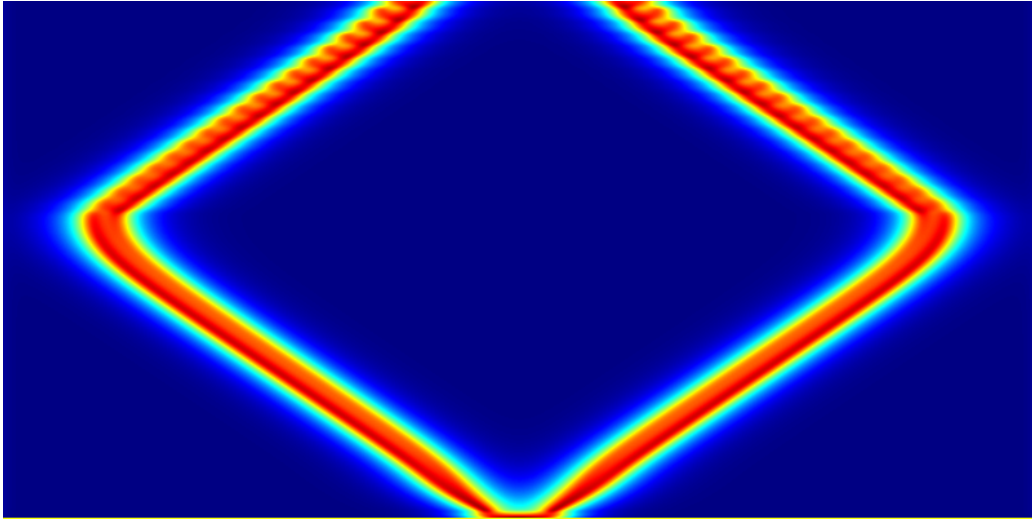(a) $\Delta t = \Delta x = 0.25$ (b) $\Delta t = \Delta x = 0.125$

(c) $\Delta t = \Delta x = 0.0625$

Figure 23. Effect of varying mesh-size on evolution of solutions to system with ramp as transition function, x-axes show distance $L = 150$, y-axes show total time $t = 800$. (a) $\Delta t = \Delta x = 0.25$, reflecting boundary conditions. (b) $\Delta t = \Delta x = 0.125$, reflecting boundary conditions. (c) $\Delta t = \Delta x = 0.0625$, reflecting boundary conditions.

51

(a) Current and Temperature Distribution

(b) Evolution

Figure 24. (a) A snapshot at time $t = 150$ of dimensionless temperature and ratio of current. The ratio of current $u \in [0, 1]$ is not to scale in this image. (b) The evolution of the solution in time, x-axes show distance $L = 200$, y-axes show total time $t = 1600$, $\Delta t = \Delta x = 0.25$, red indicates high temperature, blue indicates low temperature. In black and white images, the portion that is moving in time is elevated heat. Note, this simulation was run with reflecting boundary conditions. In the case of periodic boundary conditions, the solitons are still repelled at the boundary, but they are closer to the edges when they are repelled.
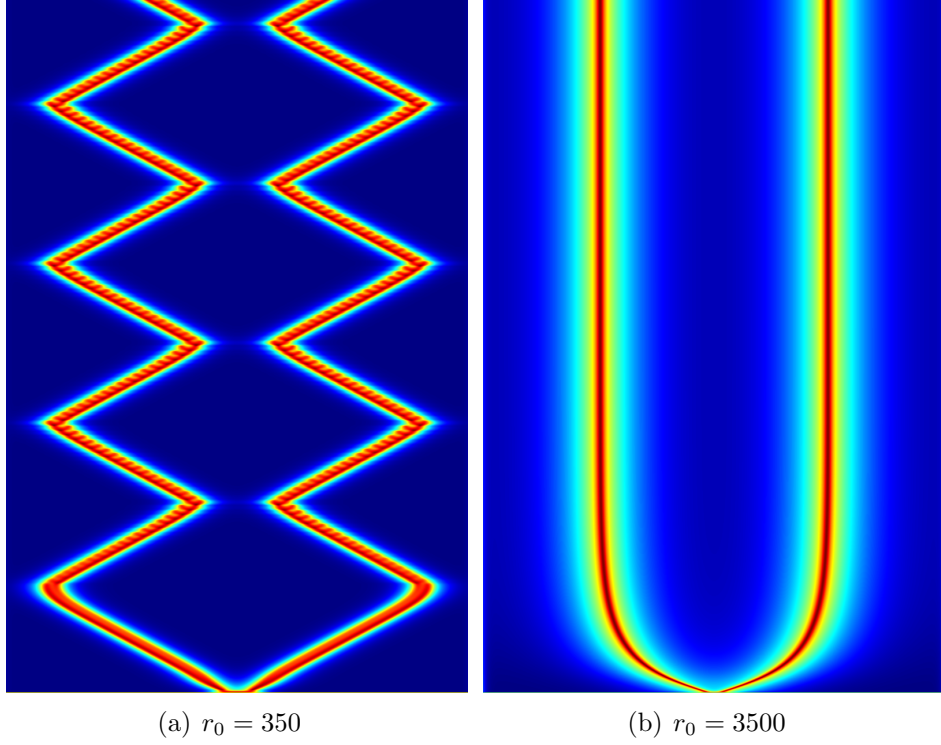
(a) $r_0 = 350$ (b) $r_0 = 3500$

Figure 25. **Effect of varying interfacial resistance , x-axes show distance $L = 200$, y-axes show total time $t = 6000$, $\Delta t = \Delta x = 0.25$. (a) A pulsating soliton solution, $r_0 = 350$, $\kappa = 0.14$, reflecting boundary conditions. (b) A non-pulsating soliton solution, $r_0 = 3500$, $\kappa = 0.19$, reflecting boundary conditions.**

as particle-like entities [2, 13]. Observing the repulsion of two or the more complex patterns that arise as multiple solitons move and are moved around, is very similar to the behavior of particles colliding, complete with a suggestion of conservation of momentum. Solutions in this region display oscillating and bounded values of $\max(\theta)$, total heat, and total variation.

4.7 Region V

Region V is the set of κ and r_0 for which a temperature profile $\theta(x, t)$—starting with the Gaussian distribution—will reshape and then resolve into a stationary soliton. This reshaping begins with the peak of the soliton dropping faster than the sides. This produces a distribution of θ with two peaks that will draw together. Figure 26(a) on the following page shows the distribution of θ for $\kappa = 0.17$ and $r_0 = 400$ at time $t = 150$ after the stationary soliton has formed. Before the peaks touch, the midpoint of the soliton will push back up and stabilize. The heating and cooling forces are balanced in such a way that a stable stationary soliton is sustained in the original position. The interfacial resistance coupled with the steep gradient term in the $r(u_x)^2$ term of (1) is strong enough that it prevents the otherwise powerful cooling term due to relatively large κ from overcoming the weak heating terms. The solutions in this region display constant values of $\max(\theta)$, total heat and total variation after the initial evolution.

4.8 Region VI

Region VI is the set of κ and r_0 for which a temperature profile $\theta(x, t)$—starting with the Gaussian distribution—decays to a uniform distribution given by the ambient temperature $\theta(x, t) = \theta_0$. Physically, this means that a perturbation in temperature vanishes. The region is characterized by large cooling parameters κ and moderate
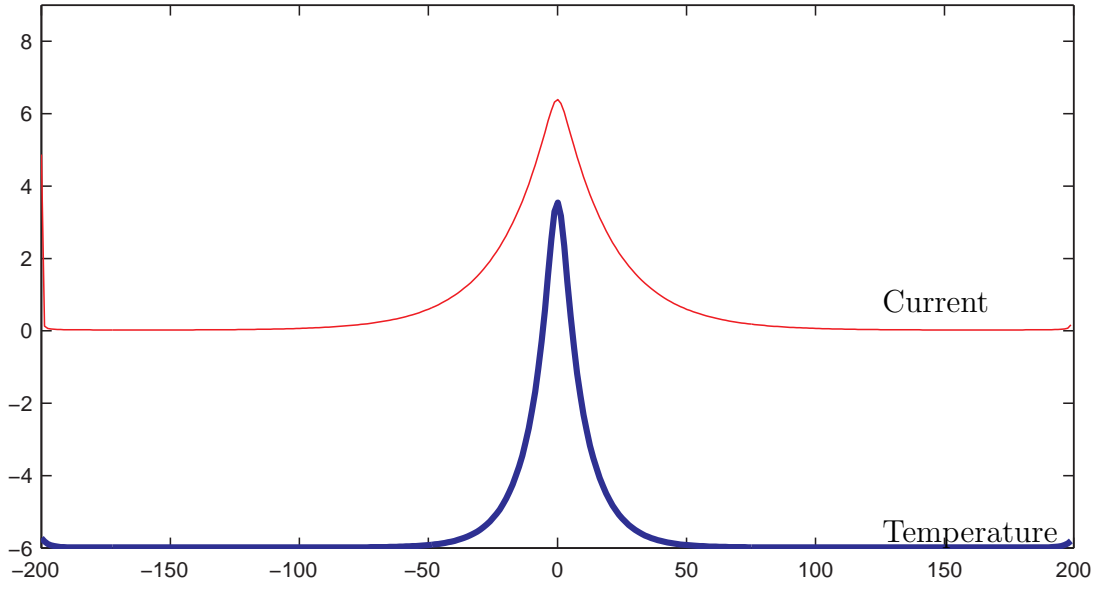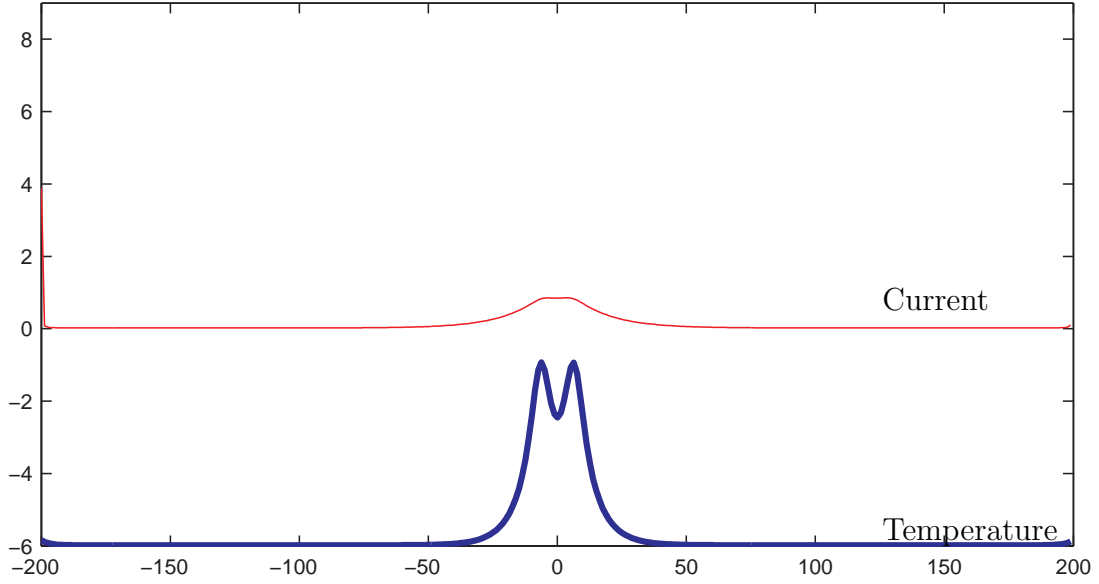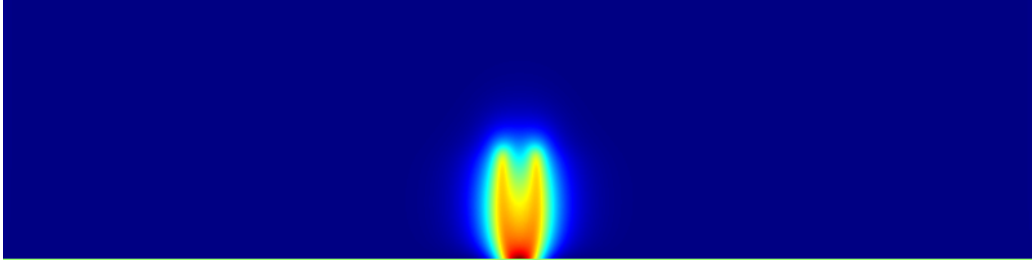
(a) Current and Temperature Distribution
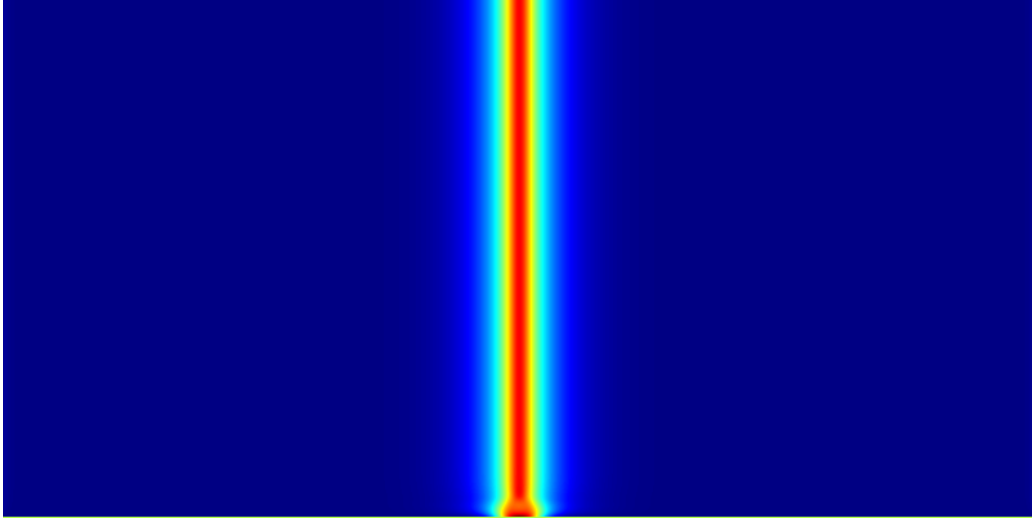
(b) Evolution

Figure 26. (a) **A snapshot at time** $t = 150$ **of dimensionless temperature and ratio of current. The ratio of current** $u \in [0, 1]$ **is not to scale in this image.** (b) **The evolution of the solution in time, x-axes show distance** $L = 200$**, y-axes show total time** $t = 400$**,** $\Delta t = \Delta x = 0.25$**, red indicates high temperature, blue indicates low temperature. In black and white images, the vertical bar in the middle of the image is elevated heat.**

55

(a) Current and Temperature Distribution

(b) Evolution

Figure 27. (a) **A snapshot at time** $t = 42.5$ **of dimensionless temperature and ratio of current. The ratio of current** $u \in [0, 1]$ **is not to scale in this image.** (b) **The evolution of the solution in time, x-axes show distance** = 400 (x/l_T), **y-axes show total time** = 100 (γt), $\Delta t = \Delta x = 0.25$, **red indicates high temperature, blue indicates low temperature. In black and white images, the portion that disappears over time is elevated heat.**

56

to low interfacial resistivity r_0. This is the only region that does not show a failure due to heating, because given sufficient cooling capacity, any heat that develops is diffused and absorbed by the coolant. Figure 27(a) on the previous page shows the temperature for $\kappa = 0.132$ and $r = 200$ at time $t = 42.5$ after it has dropped below the current sharing temperature $\theta = 0$. Because κ is large, the cooling term $\kappa(\theta - \theta_0)$ dominates the heating terms of (1) near the center of the Gaussian distribution where the temperature is highest. This causes the peak to decay quickly. Because the interfacial resistance is sufficiently strong, the higher current gradients on either sides of the peak contributes to heating which counteracts the cooling, resulting in the dual peak distribution shown in Figure 27. The temperature continues to decay in time asymptotically approaching a uniform distribution at the ambient temperature. For a lower interfacial resistivity, $\kappa = 0.18$ and $r_0 = 50$ for example, the heat diffuses more uniformly in space and there is only a subtle change in shape of the temperature profile from the Gaussian distribution as it shrinks until it disappears.

V. Conclusion and Areas for Further Research

5.1 Conclusion

This thesis has explored the similarities and differences between a model for heat and current in a superconducting wire and a similar model for a hyper-conducting wire. In each case there are solutions characterized by heat gain and heat loss. The solutions characterized by heat gain describe a type of failure in the wire. By increasing interfacial resistance between the superconductor and the stabilizer it is possible to increase the likelihood of detecting one of these failures before critical damage is done to the system. The differences in the models considered are largely a matter of scale in terms of both spacial domain and time. In the superconducting wire, the transition to normal conductivity occurs over a much smaller temperature range than in the hyper-conducting wire. This changes the scale and temperature ranges of some of the solutions but does not change the qualitative nature of the solutions. All research conducted in conjunction with this thesis was limited to the one dimensional model with constant interfacial resistance. Expanding these parameters provides material for further research.

5.2 Varying Interfacial Resistance

It is possible to vary the interfacial resistance in the domain $x \in [-L, L]$. Primarily this system has been studied with a uniform resistivity over the domain with lowest resistivity at the boundaries. Instead, consider the interfacial resistance as a series of wells in an otherwise high level of interfacial resistance. This is a reasonable simulation of a change to the physical wire. In the original case, consider a continuous wire with uniform resistive layer applied between the YBCO and the copper. This case would be analogous to placing several breaks in the resistive layer along the length of the

58

wire. Such a change would likely slow the speed of normal zone propagation, but it might also allow for better dissipation and more stability since the resistivity is one of the factors that contributes to normal zone propagation. The original expression for interfacial resistance is

$$r(x) = \epsilon + r_0 \left(1 - e^{(\cos(x\pi/(2L)))^2/c^2}\right).$$

The simplest approach to modify $r(x)$ is to change the coefficient of x in the cosine term

$$r(x) = \epsilon + r_0 \left(1 - e^{(\cos(nx\pi/(2L)))^2/c^2}\right)$$

where $n \in \mathbb{Z}^+$.

5.3 Two-Dimensional Model

The one dimensional model is sufficient for initial exploration and describing a length of wire. It is not appropriate for modeling a coil of wire like the ones used for electromagnets. In that case, since there is heat transfer between layers, but no current between layers, the model would need to be modified and or extended.

5.4 Transition Function

Consider the resistance of aluminum shown in Figure 7 on page 16. Rather than exponential, this appears asymptotically linear. With that in mind, a hyperbolic function might be more appropriate. It might prove illuminating to implement a function like

$$f(\theta) = \sqrt{\theta^2 + 1} - 1$$

instead of the exponential function.

59

Bibliography

[1] N. Akhmediev and A. Ankiewicz, editors. *Dissipative solitons*, volume 661 of *Lecture Notes in Phys.* Springer, Berlin, 2005.

[2] M. Bode, A. W. Liehr, C. P. Schenk, and H. G. Purwins. Interaction of dissipative solitons: particle-like behaviour of localized structures in a three-component reaction-diffusion system. *Physica D: Nonlinear Phenomena*, 161(1–2):45–66, 2002.

[3] P. D. Desai, H. M. James, and C. Y. Ho. Electrical resistivity of aluminum and manganese. *Journal of Physical Chemistry Reference Data*, 13(4), 1984.

[4] S. V. Gurevich, Sh. Amiranashvili, and H. G. Purwins. Breathing dissipative solitons in three-component reaction-diffusion system. *Physical Review E (Statistical, Nonlinear, and Soft Matter Physics)*, 74(6):066201, 2006.

[5] L. Hampton, P. N. Barnes, T. J. Haugan, G. A. Levin, and E. B. Durkin. Compact superconducting power systems for airborne applications. *Weapon Systems Technology Information Analysis Center Quarterly*, 9(1), 2009.

[6] E. Knobloch. Spatially localized structures in dissipative systems: open problems. *Nonlinearity*, 21(4):T45–T60, 2008.

[7] G. A. Levin. Personal interview. Conversation on 14 October 2009.

[8] G. A. Levin, P. N. Barnes, and K. A. Novak. The effects of superconductor-stabilizer interfacial resistance on quench of current-carrying coated conductor. *Superconductor Science and Technology*, 23, 2010.

[9] G. A. Levin, P. N. Barnes, J. P. Rodriguez, J. A. Connors, and J. S. Bulmer. Emergence of dissipative structures in current-carrying superconducting wires. *Physical Review E (Statistical, Nonlinear, and Soft Matter Physics)*, 79(5):056224, 2009.

[10] K. W. Morton and D. F. Mayers. *Numerical Solution of Partial Differential Equations: An Introduction.* Cambridge University Press, New York, NY, USA, 2005.

[11] A. Quarteroni, R. Sacco, and F. Saleri. *Numerical Mathematics (Texts in Applied Mathematics).* Springer-Verlag New York, Inc., Secaucus, NJ, USA, 2006.

[12] B. Raveau, C. Michel, M. Hervieu, and D. Groult. *Crystal chemistry of high Tc superconducting copper oxides*, volume 15 of *Springer series in materials science.* Springer-Verlag, Berlin, 1991.

[13] C. P. Schenk, P. Schütz, M. Bode, and H. G. Purwins. Interaction of self-organized quasiparticles in a two-dimensional reaction-diffusion system: The formation of molecules. *Phys. Rev. E*, 57(6):6480–6486, Jun 1998.

[14] Constance E. Schuster, Mark G. Vangel, and Harry A. Schafft. Improved estimation of the resistivity of pure copper and electrical determination of thin copper film dimensions. *Microelectronics Reliability*, 41(2):239 – 252, 2001.

[15] T. Sekitani, N. Miura, S. Ikeda, Y. H. Matsuda, and Y. Shiohara. Upper critical field for optimally-doped $YBa_2Cu_3O_{7-\delta}$. *Physica B: Condensed Matter*, 346–347:319–324, 2004. Proceedings of the 7th International Symposium on Research in High Magnetic Fields.

[16] W. Yu, F. Yao, and D. Yang. Critical points of a non-linear functional related to the one-dimensional Ginzburg-Landau model of a superconducting-normal-superconducting junction. *Nonlinear Analysis: Theory, Methods and Applications*, 68(7):2038–2057, 2008.

1. REPORT DATE *(DD-MM-YYYY)* 11-12-2009	2. REPORT TYPE **Master's Thesis**	3. DATES COVERED *(From – To)* Mar - Dec 2009

4. TITLE AND SUBTITLE	5a. CONTRACT NUMBER
Heat and Current Propagation in Buffered Superconducting and Hyper-conducting Wire	5b. GRANT NUMBER
	5c. PROGRAM ELEMENT NUMBER
6. AUTHOR(S) Lynn, Jesse L. Captain, USAF	5d. PROJECT NUMBER
	5e. TASK NUMBER
	5f. WORK UNIT NUMBER

7. PERFORMING ORGANIZATION NAMES(S) AND ADDRESS(S) Air Force Institute of Technology Graduate School of Engineering and Management (AFIT/EN) 2950 Hobson Way, Building 640 WPAFB OH 45433-8865	8. PERFORMING ORGANIZATION REPORT NUMBER AFIT/GAM/ENC/09-02
9. SPONSORING/MONITORING AGENCY NAME(S) AND ADDRESS(ES) N/A	10. SPONSOR/MONITOR'S ACRONYM(S)
	11. SPONSOR/MONITOR'S REPORT NUMBER(S)

12. DISTRIBUTION/AVAILABILITY STATEMENT
   APPROVED FOR PUBLIC RELEASE; DISTRIBUTION UNLIMITED.

13. SUPPLEMENTARY NOTES

14. ABSTRACT
This research models and analyzes the distribution of heat and current in a buffered superconducting or hyper-conducting wire that shows potential for use in different capacities in multiple Air Force systems including the Active Denial System. The thesis includes a brief background of the reaction-diffusion system of partial differential equations provided by AFRL/RZPG and development of the numerical scheme. It then explores solutions to the model. These solutions indicate some of the various heat-related failures that may be observed in such a wire. The nature of the solutions observed depends on the characteristics of the wire, operating temperature and efficiency of cooling.

15. SUBJECT TERMS
   Superconductor, YBCO, dissipative soliton, reaction-diffusion, partial differential equation

16. SECURITY CLASSIFICATION OF:			17. LIMITATION OF ABSTRACT	18. NUMBER OF PAGES	19a. NAME OF RESPONSIBLE PERSON Kyle A. Novak, Lt Col, Phd, AFIT
REPORT U	ABSTRACT U	c. THIS PAGE U	UU	70	19b. TELEPHONE NUMBER *(Include area code)* 937-255-3636 x4635e-mail: kyle.novak@afit.edu